Measurement 254 (2025) 117655

Contents lists available at ScienceDirect

Measurement

journal homepage: www.elsevier.com/locate/measurement

A survey on inline soil pollution measurement and mapping technologies

Valerio Brunacci [d], Domenico Capriglione [b], Chiara Carissimo [c], Damiano Crescini [a], Filippo Milano [b], Nicola Moggia [a], Antonio Moschitta [d,*], Giorgia Polidori [a], Cecilia Provenzale [b], Francesco Santoni [d], Emilio Sardini [a], Mauro Serpelloni [a]

[a] Department of Information Engineering, University of Brescia,, Via Branze, 38, 25123 Brescia (BS), Italy
[b] Department of Electrical and Information Engineering, University of Cassino and Southern Lazio, Via di Biasio n. 43, 03043 Cassino (FR), Italy
[c] Department of Medicine and Health Sciences "V. Tiberio", University of Molise, Via Francesco De Sanctis s.n.c., 86100 Campobasso (CB), Italy
[d] Department of Engineering, University of Perugia, Via G. Duranti 93, 06125 Perugia (PG), Italy

ARTICLE INFO

Keywords:
Underground
Measurement
Positioning
Sensors
Assessment
Pollution
Monitoring

ABSTRACT

This paper reviews recent advancements in underground positioning and monitoring, particularly for soil pollution detection and mapping. Unlike conventional indoor and outdoor systems, underground environments pose unique challenges. Robotic platforms, including the Moon/Mars Underground Mole (MMUM) and bioinspired Mole-bot, utilize drills, augers, and additive layering for soil exploration, with some featuring autonomous control for efficient data collection. The review also examines real-time soil monitoring techniques, such as electrochemical sensors for pollutant detection and spectroscopic methods like Laser-Induced Breakdown Spectroscopy (LIBS) and Near-Infrared Reflectance Spectroscopy (NIRS). These approaches, when combined, enhance large-scale soil analysis for environmental and agricultural applications. Additionally, underground positioning remains complex due to electromagnetic interference and GPS unavailability. Techniques like Ground Penetrating Radar (GPR), ultra-wideband (UWB), ZigBee, and magnetic field-based localization provide potential solutions but face limitations such as signal attenuation. Continued research is essential for improving the accuracy and efficiency of these methods in subsurface applications, from pollution monitoring to resource exploration.

Contents

1. Introduction 2
2. Inline solutions with autonomous robots 3
3. Inline pollution measurement methods 4
   3.1. Inline methodologies using electrochemical sensors 4
   3.2. Inline methodologies using near infrared reflectance spectroscopy (NIRS) and laser-induced breakdown spectroscopy (LIBS) 6
4. Inline mapping methods 8
   4.1. Electromagnetic compatibility issues in underground scenarios 8
   4.2. Advanced underground positioning techniques 8
      4.2.1. Ground penetrating radar 9
      4.2.2. Radiofrequency 10
      4.2.3. Magnetic fields 10
   4.3. Magnetic field sensors 11
5. Discussion and conclusions 13
CRediT authorship contribution statement 14
Declaration of competing interest 14
Acknowledgments 14

* Corresponding author.
E-mail addresses: valerio.brunacci@unipg.it (V. Brunacci), capriglione@unicas.it (D. Capriglione), chiara.carissimo@unimol.it (C. Carissimo), damiano.crescini@unibs.it (D. Crescini), filippo.milano@unicas.it (F. Milano), nicola.moggia@unibs.it (N. Moggia), antonio.moschitta@unipg.it (A. Moschitta), giorgia.polidori@unibs.it (G. Polidori), cecilia.provenzale@unicas.it (C. Provenzale), francesco.santoni@unipg.it (F. Santoni), emilio.sardini@unibs.it (E. Sardini), mauro.serpelloni@unibs.it (M. Serpelloni).

https://doi.org/10.1016/j.measurement.2025.117655
Received 27 January 2025; Received in revised form 9 April 2025; Accepted 20 April 2025
Available online 6 May 2025

Data availability 14
References 14

1. Introduction

Soil contamination refers to the presence of harmful substances in the soil, typically resulting from human activities such as industrial operations, agricultural practices, or improper disposal of waste. This happens when contaminants spread, emit, transform, and dilute in other mediums before eventually settling in the soil. As a result, the relationship between the source of the contaminants and the extent and severity of soil contamination is not well defined. This type of contamination is often linked to atmospheric deposition, certain agricultural practices, inadequate recycling and treatment of waste and wastewater, and natural events like floods and landslides. Human-made contaminants, such as nutrients and acid deposition, enter the atmosphere through emissions from industries, transportation, households, and agricultural activities. Some agricultural practices lead to diffuse soil contamination by directly applying pesticides, sewage sludge, compost, fertilizers, and manure. Currently, significant problems arising from diffuse sources include acidification, nutrient surplus impacts, and heavy metal contamination [1]. Localized soil contamination results from intensive industrial activities, improper waste disposal, mining, military operations, or accidents, introducing high levels of contaminants into the environment. Even within presently functioning industrial sites, soil contamination might have historical roots, yet ongoing operations still wield considerable influence [2].

Various soil pollutants are mainly divided into two categories: organic and inorganic, both of which come from various human activities such as industry, agriculture, urban areas, and waste disposal. Organic pollutants include petroleum-derived compounds such as benzene, toluene, ethylbenzene and xylene (known as BTEX), polycyclic aromatic hydrocarbons (PAHs), pesticides and herbicides such as organophosphates and glyphosate. Other examples include organochlorine compounds such as PCBs and CFCs, and industrial solvents such as trichloroethylene (TCE) and tetrachloroethylene (PCE). Inorganic pollutants include heavy metals such as lead, mercury, cadmium, arsenic, chromium, and copper, which contaminate soil due to industrial activities, waste discharges, and the use of fertilizers and pesticides. Lighter metals such as aluminum and magnesium are also present in the soil in the form of minerals and inorganic compounds. In addition, there are soluble inorganic compounds such as nitrates, sulfates, phosphates and chlorides, and chemicals such as ammonia, sulfuric acid and hydrochloric acid. Combustion residues such as ash and soot can contain nitrogen, sulfur and carbon oxides, while construction materials such as cement, concrete, ceramics and glass can also be sources of inorganic pollution.

Soil pollution can significantly affect the soil's functionality. It can hinder the support of vegetation growth and biomass production; limit the provision of essential materials and substrates for human activities, ecological systems, and nutrient cycling. Additionally, it may impair the soil's ability to filter and buffer, leading to consequences in the hydrosphere, endangering groundwater reservoirs, and posing risks to aquatic life. As a precautionary measure, regulations for assessing contamination were devised, with a focus on health guidelines. Contamination can either occur broadly across an area or be concentrated in specific locations [3,4]. Both phenomena need to be properly addressed.

This survey paper explores the latest developments in environment positioning, sensors, and monitoring scenarios, focusing on shallow soil scenarios that are more difficult to be identified. By mimicking the role of Unmanned Aerial Vehicle (UAV) in monitoring the spread of phenomena like forest fires, an interesting solution is the deployment of underground or underwater drones, which may directly access the corresponding environment and provide real-time measurements taken on the spot. To this aim, both advanced sensors and positioning systems are required, complying with requirements specific for the selected application, measurand quantity, and environmental characteristics. While there is currently a strong emphasis on indoor or outdoor positioning systems, positioning techniques in difficult environments like underground or underwater are less developed. It is worth noting that availability of timely and accurate measurements may provide situational awareness and may permit a quick and effective reaction to disasters or emergencies, reducing the response time and ensuring rational decisions based on reliable data. While deep underground scenarios are interesting for mining activities for geological prospections, shallow depth soil monitoring appears a promising field of investigation, since they are reachable by autonomous or remotely controlled unmanned vehicles, and because this depth is most related to typical human activities, including storage and management of industrial byproducts and wastes.

The identification of pollutants in the soil is therefore an important task. The classic method requires a laboratory analysis of the collected samples. This off-line soil analysis begins with the collection of soil samples using standardized techniques, followed by laboratory testing to measure parameters like pH, nutrient content, heavy metals, and organic matter. Common methods include spectroscopy, chromatography, and mass spectrometry. The main advantages of off-line methodologies are their high accuracy and precision, allowing for comprehensive analysis of multiple soil parameters at once. This holistic approach helps researchers understand soil health, fertility, and contamination, especially in complex soil matrices. However, off-line methods have notable drawbacks, including being time-consuming and resource-intensive, requiring specialized equipment and trained personnel. The process can lead to delays in results, and inherent spatial and temporal variability in soil samples may introduce biases, affecting data reliability. Additionally, off-line analysis often lacks the spatial resolution needed for detailed assessments across larger areas. Therefore, in this survey paper, in-line methods are studied aiming at measuring pollutants directly in the soil and at the same time mapping the area under observation. Examples of in-line soil analysis methods are those incorporating electrochemical sensors and near-infrared (NIR) spectroscopy. These innovative methodologies offer real-time, on-site assessment of soil parameters, revolutionizing traditional soil analysis practices. Moreover, they offer the advantage of providing immediate feedback and continuous monitoring, allowing for timely interventions and informed decision-making.

The other aspects that must be considered when using these in-line methods are the mapping and localization systems. Underground localization presents unique challenges due to GPS inaccessibility, signal attenuation, and environmental heterogeneity. This paper reviews advanced positioning techniques, including ultrasound [5–7], Ground Penetrating Radar (GPR) [8], radio frequency (RF) [9], and magnetic field methods [10]. As better highlighted in the following, ultrasound-based systems, often combined with vision or electromagnetic sensors, enable accurate tracking in confined spaces. GPR excels in subsurface mapping but is limited by system size and cost. RF technologies, such as ultra-wide band (UWB), offer precise localization but require dense sensor networks. Magnetic field methods, leveraging anomaly detection and artificial fields, provide non-invasive, high-accuracy solutions for different applications, including buried object detection and animal tracking. A comparative analysis highlights the trade-offs in performance, cost, and domain suitability, offering insights for selecting optimal approaches in underground environments. The specific application also highlights the need for robotic systems to move underground

and measure pollution. The state of art presents several robotic solutions for underground exploration even if, in these systems, there is an absent or poor analysis of the soil (i.e., RAMAN Spectrometer, soil temperature, and soil humidity). This paper reviews some robotic platforms developed for underground exploration, comparing their motion modules, structure parameters, excavation tests performance, and soil analysis module whenever present. The rest of the paper is organized into three chapters. In the second chapter, inline solutions with autonomous robots are presented and analyzed. In the third chapter, inline measurement methods and in the last chapter, inline mapping techniques are reported. The aim is to analyze in all its components the potential systems for the identification and mapping of pollutants in the soil and to provide the scientific community with design methodologies, awareness of available degrees of freedom, and tools for the study and development of these important autonomous measurement systems.

2. Inline solutions with autonomous robots

Underground soil exploration is useful in different application fields like finding new subsoil sources (i.e., petroleum, coal, water) [11–15], geotechnical investigations [16,17], pipes installations (i.e., communication, power, water) [18,19] or subsurface exploration missions (e.g., lunar or mars missions) [20–28]. The use of robotic systems has different advantages like the exploration of risk environments or inaccessible for humans [29,30] as well as video surveillance [31]. Future developments in robotic systems for underground exploration could benefit from emerging technologies such as flexible and fibric electronic sensors for environmental monitoring [32,33]. These novel technologies may be quite useful for building bioinspired flexible or reshapeable robots, eventually operating in mixed environments. The state-of-the-art presents a few examples of underground robotic platforms used for soil analysis and measurements of specific quantities [14,15,27,28]. For this reason, this section aims to describe the robotic solutions generally developed for underground soil explorations, comparing their main characteristics. Furthermore, such an analysis can provide helpful information for designing an autonomous underground robot that can also provide an inline soil analysis. Several robotic platforms have been developed for Mars and Lunar missions' purposes. For example, the Moon/Mars Underground Mole (MMUM) has been designed for planetary subsurface exploration integrating a Raman Spectrometer, a temperature sensor, and a space in the tip to collect soil samples (i.e., about 7 g) [27,28]. The MMUM exploits a hammering technique to penetrate the soil. Indeed, the robot includes a motor and a gearhead system to compress a spring and to release it on a striking mass. Unfortunately, the system requires additional surface components making the whole platform cumbersome. The MMUM allows to perform only vertical soil exploration, and it can be controlled in teleoperation modality through a Linux/Window GUI. The authors in [29,30] propose a low-cost drilling robot that tries to reduce the dimensions of the whole system by embedding a power supply (allowing an autonomy of 57 min) but at expense of soil analysis sensors and sample collection modules. The structure of the robot includes a motor, an epicyclic gearing to control the robot screw and two anti-torque panels. Differently from the previous solutions, in order to provide the robot of a locomotion and steering module, the authors in [31] propose the use of four vertical drills placed at the corner of a rectangular frame (i.e., Quad digger robot). This robot is able to bury itself as well as to move on the surface when the four drills are rotated 90° with respect to the frame. The Quad digger is not able to change modality autonomously but the four drills can be controlled independently to modify the robot orientation, using a C++/Qt GUI. The user can control the motor direction and speed of each drill. The Quad digger does not include embedded sensors or power supply, but the authors suggest the use of the space inside the drills to accommodate them. The DIGBOT robot shown in [17] also implements a drill tip but differently from the previous solution, it proposes a contra-rotating tip to reduce the counter force from soil. The tip is composed of two parts that rotate in opposite directions using a planetary gear in the upper section. The excavation tests performed on Polypropylene (PP) pellet showed a penetration rate equal to 114 mm/min even if they highlighted the lack of a proper locomotion module. For this reason, Gu et al. in [16] present a snake-robot that could be attached to the DIGBOT to overcome this limit. The system is composed of 6 servo motors and a metal plate to provide locomotion and an anchoring mechanism. Notwithstanding the encouraging preliminary results, no tests have been conducted on integration with DIGBOT. The authors in [16] are not the only ones that took inspiration from nature for designing their robot systems. Indeed, in [20–22] the authors propose a peristaltic crawling robot bioinspired to worm movement. The robot has a locomotion and an excavation module. The first one is constituted by four subunits. Each of them includes two stepper motors that control the extension as well as the contraction of dual pantographs to reproduce a peristaltic movement. The excavation module includes an earth auger to penetrate the soil and to transport the excavated material behind the robot. Another robot bioinspired by inchworm movement is the BADGER robot [18,19] that differently from the previous solution also includes a steering module. This system is composed of three modules: (i) a drill-head to excavate into the soil, that also includes Ground Penetrating Radar components (GPR) to avoid obstacles like buried tubes [34]; (ii) a service module that embeds pneumatic, hydraulic and electrical motors and an airbag whose expansion/compression allows robot clamping and locomotion; and (iii) a joint module equipped with pneumatic cylinders to steer the robot (see Fig. 1). The desired linear and rotational speed of the drill-head can be controlled using a teleoperation interface but no data on excavation tests are available. The Inchworm Boring Robot (IBR) is another robot that employs a peristaltic movement to penetrate the ground, and it has been designed for the exploration of the lunar soil [24–26]. Differently from BADGER it does not have a steering module but includes a module for samples soil collection and has a lower dimension. The system is composed of a drilling module and a chip removal device (CRD) for transporting soil samples and supporting the system during the excavation procedure. The drilling module includes a drill to break the soil and an auger to move the cuttings to another contra-rotating auger (i.e., discharging module) and towards the CRD. A propulsion module controls the linear motion between the excavation and the discharging module. The IBR can be controlled through a Matlab/Simulink GUI. A totally different approach to explore the ground is proposed by [14,15]. The authors proposed a robot system (i.e., a robot plant) that grows in the soil using an additive layering technique and replicates the gravitropic and hydrotropic root behavior. The robot plant exploits a filament, a motor, a gear transmission system, and a nozzle to increase the root dimension and to penetrate the soil. The robot apex includes an accelerometer and a humidity sensor to automatically steer the system towards the gravity and water sources. The results showed a successful replication of the real apex behavior even if this approach requires a growth of the robot equal to the desired penetration depth and it does not consider a mechanism to retrieve it. Another approach to search new subsoil sources is proposed in [11–13,35]. The authors present the Mole-bot, a robot bioinspired from diggers animals like the European mole and the African mole-rat. The Mole-bot implements an expandable drill tip and a forelimb mechanism that allow it to penetrate the soil and to remove the excavated respectively. The system allows drilling holes of 93.4 mm in non-expanded mode and of 202 mm in the expanded modality. The robot also implements a steering module with an elastic joint and two linear actuators. The first version of the locomotion module combined legs and expandable mechanisms to lock the robot against the wall while the third version of Mole-bot adopts three caterpillar wheels (see Fig. 2). These last are placed at the vertices of a triangle to support the robot structure in the underground holes. The robot movement (i.e., forward, backward, left, and right direction), the drill, and the discharging modules can

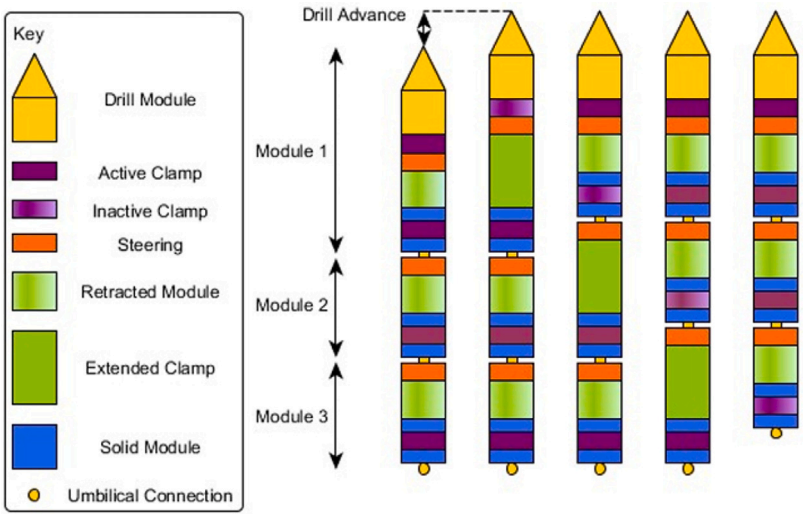

Fig. 1. BADGER robot [40].

be controlled in teleoperation modality. The Mole-bot is able to localize itself through 3D Simultaneous Localization and Mapping (SLAM) technology [36–38]. The latter creates a map of the Earth's magnetic field, and the robot localizes itself by performing a re-measurement of the magnetic field and finding similarities with the data previously collected. Indeed, the Mole-bot implements two magnetic sensors: both in forward and backward movement the second sensor will measure the same magnetic field sequence as the previous one allowing the robot self-localization. The test performed on a ramp of 5 m length and 6° showed an error of 0.13 m with respect to the ground truth; however, no data on tests performed in an underground environment are available.Recently, the same approach has been adopted by other authors in [39]. They proposed another robot bioinspired by the European mole structure that can burrow and crawl. The robot is divided into three modules: (i) the head; (ii) the chest where the forelimb mechanism is attached, and (iii) the hip with a hindlimb mechanism. The latter facilitates soil remotion and contributes to robot locomotion with the head and the forelimb mechanism. The authors developed three head shapes and tested the robot burrowing capabilities in polypropylene plastic particles. The penetration tests showed a robot speed of about 40.4 mm/min in the best combination of head shape and forelimb mechanism movement. However, this system does not present a proper drilling module, limiting its application in the real environment. Moreover, the authors highlighted different limitations in robot burrowing capabilities, raising the need to investigate the mechanical interaction between soil mechanics properties and robot structure in-depth. This analysis, in combination with gain optimization, will allow the estimate of the robot's energy consumption and facilitate it in unstructured and complex soil environments

Table 1 compares the mentioned solutions with respect to their motion structure and soil analysis module (if present). The robot structure can be split into four modules: (i) drill module to perforate the soil; (ii) discharging module to remove the cutting materials; (iii) locomotion module to move the robot forward or backward; and (iv) steering module to direct the robot in different directions. It is possible to observe how for mars and lunar missions, the robotic solution is designed without a steering module. Indeed, it is usually required to perform only vertical perforation to collect soil samples [23–28] or to perform soil analysis [27,28]. Differently, in applications like service pipe installation or subsoil sources research, it is required to provide the robot with a steering module to allow the navigation in the ground. These robotic solutions usually can be controlled by a human user through ad-hoc GUI, except for the robot plant that implements an autonomous control based on gravity and soil humidity data. The Mole-bot solution has a complete motion assembly, and it is the only one that implements SLAM (Simultaneous Localization and Mapping) technology to localize itself.

Table 2 shows the size of the robots and the excavation test data. The penetration rate parameter is influenced by the material used in the test as well as the robot dimension and the type of drill tip. Indeed, due to the several applications, different tested materials with specific density and granular dimensions have been adopted. As described previously, the mentioned robot solutions adopt different methods to penetrate the ground: drill tip (i.e., MMUM, Quad Digger, Badger, IBR, Mole-bot), contrarotating drill (i.e., DigBot), auger (i.e., screw-driven robot, peristaltic crawling robot), and additive layering technique (i.e., Robot Plant). Moreover, the penetration rate is influenced by the presence of a locomotion and discharging module that facilitate the robot movement in the ground, increasing the achievable depth but at the expense of excavation time due to the activation of the different modules in sequence (e.g., see Mole-bot). This analysis shows that BADGER and Mole-bot robots represent the most complete solution for underground navigation. However, no data on the penetration rate are available for the BADGER, while only tests in the laboratory were performed for Mole-bot. Moreover, an energy consumption of 7–8 kW has been estimated for the BADGER [40]. These aspects can affect the actual application of these solutions in real scenarios.

3. Inline pollution measurement methods

In the literature, two main methods are viable when inline pollution measurements are requested. This chapter provides an overview of inline real-time electrochemical sensors and NIR spectroscopy techniques for soil analysis, elucidating their principles, applications, and potential benefits across various domains.

3.1. Inline methodologies using electrochemical sensors

Electrochemical sensors enable inline analysis for real-time monitoring of chemical and physical parameters in shallow soil. This advanced approach is widely used in industries such as agriculture, environmental monitoring, and natural resource management. In particular, these sensors are widely used for environmental parameters because they enable the detection of harmful pollutants and gases in the soil [1,2]. There are various types of electrochemical sensors that result in different measurements, including amperometric, potentiometric or conductimetric. Amperometric sensors are used to detect the level of available oxygen in the soil. This is important for the

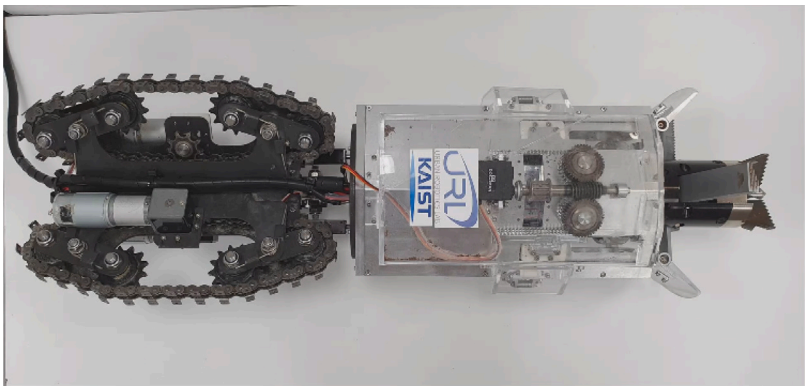

Fig. 2. Mole-bot robot (third version) [35].

Table 1
Summary of the identified robotic solutions with respect to their motion structure and soil analysis module. The robots are split between non bioinspired and bioinspired robots.

Robot	Motion structure				Soil analysis module	
	Drill	Discharging	Locomotion	Steering	Storage soil	Embedded sensors
MMUM	✓	×	×	×	✓	✓
Screw-driven robot	✓	×	×	×	×	×
Quad Digger	✓	×	×	✓	×	×
Digbot	✓	×	✓[a]	×	×	×
Peristaltic Crawling robot	✓	✓	✓	×	×	×
Badger	✓	×	✓	✓	×	×
IBR	✓	✓	✓	×	✓	×
Robot Plant	✓	×	✓	✓	×	✓ - Soil humidity
Mole-bot	✓	✓	✓	✓	×	×
Mole-inspired	×	✓	✓	✓	×	×

[a] Only if in combination with the snake-robot [16].

Table 2
Structure parameters and excavation test data of the mentioned robotic solutions. The robots are split into no bioinspired and bioinspired robots.

Robot	Structure parameters			Excavation test	
	Length [mm]	Diameter [mm]	Weight [kg]	Tested material	Penetration rate [mm/min]
MMUM	600	40	2	Beach sand	1.16
Screw-driven robot	204	28	0.150	Quarts sand	100
Quad Digger	270 × 270 × 190		5	Sand	600
Digbot	300	30	–	Polypropylene (PP) pellet	114
Peristaltic Crawling robot	800	130	5.6	Reddish soil	9.84
Badger	4000	250	–	–	–
IBR	500	80	3.5	Cenozoic alkaline olivine basalt	8.3
Robot Plant	–	50	–	Granular medium of polyoxymethylene plastic beads (4mm diameter)	13.8
Mole-bot[a]	840	250	26	Autoclaved lightweight concrete	17.5
Mole-inspired	224 × 127 × 75		0.524	Polypropylene plastic particles	40.4

[a] Size of the third version of Mole-bot [35].

respiration of roots and microorganisms, or to detect the presence of organic compounds participating in redox reactions [41]. Voltammetric sensors provides information about the electroactive species present and their concentrations [42]. Potentiometric sensors are used to measure pH concentrations of specific ions such as metals (Pb(II), Cu(II), Cd(II) and Zn(II)), organic pollutants or other molecules such as pesticides [43], herbicides [44] and fungicides [45]. Conductivity sensors measure the electrical conductivity of a solution, which is proportional to the total concentration of ions (salts) present. Conductivity is affected by the amount and type of dissolved salts [42]. The advantages of these sensors are various. They offer immediate measurements, allowing rapid reaction to process changes. They have high sensitivity and specificity since they can detect low concentrations of specific chemicals. In addition, they can be integrated directly into the production line without taking up much space by allowing automatic data collection and thus reducing the need for manual intervention. To date, several organic and inorganic molecules and ions have been detected, studied, and quantified: heavy metals [46,47] and light metals [48]. Among the various measurement techniques voltammetric and potentiometric ones have been mainly exploited. Various techniques were used among the organic pollutants, including

potentiometric and a particular voltammetric technique, namely Differential Pulse Voltammetry (DPV). Using potentiometric techniques, herbicides and fungicides were studied. In [49], the authors utilized an All-Solid-State Ion-Selective Electrode (ASS-ISE) with an ion-selective membrane (ISM) made of polyvinyl chloride (PVC). The membrane contained molecularly imprinted polymer (MIP) nanospheres, which function as receptors for the selective detection of bispyribac.

A polyaniline film (PANI) was also embedded to act as a solid contact on the electrode. In contrast, in [50], five new potentiometric membrane sensors for determination of dinotefuran levels in cucumber and soil samples were developed. Four of these sensors were based on a newly developed molecularly imprinted polymeric material (MIP) consisting of acrylamide or methacrylic acid as a functional monomer in a plasticized PVC (polyvinyl chloride) membrane before and after pattern elution. A fifth sensor based on carboxylated PVC plasticized with dioctylphthalate was also prepared and tested. A glassy carbon electrode modified with gadolinium niobate nanoparticles (GdNbO4) was studied with DPV and used as a sensor to detect and determine aclonifen herbicide [51]. Square Wave Anodic Stripping Voltammetry (SWASV) and potentiometry were used for heavy metal detection. For the former technique, several sensors all directed towards heavy metals of different types were used. A PVC Screen-Printing Electrode (SPE) modified with Fe-Chitosan was used for the detection of arsenic [52]. Cadmium ion was also studied and detected by the same technique by a disposable screen-printed electrode (SPE) modified with ionic liquid (IL) n-octylpyridinium hexafluorophosphate (OPFP) and graphene (GR) fabricated and used for sensitive detection of Cd (II) in trace soil. Only lead was evaluated through a synthesis of a layered nanocomposite that has the structure of a three-layer "sandwich": gold nanoparticles (AuNPs), polypyrrole (PPy) and titanium disulfide (Ti3C2Tx). To improve the stability and electrochemical properties of the resulting material, 2D MXenes (such as titanium disulfide) were incorporated into a matrix of more stable materials (such as gold nanoparticles) in order to improve the electrical conductivity through polypyrrole [53]. The heavy metal Pb(II) was detected through a special electrode fabricated by in situ plating of bismuth ions on the surface of SWCNTs-Nafion/IL/SPE: this is a screen-printed electrode (SPE) modified for sensitive detection of trace amounts of lead (Pb(II)). SWCNTs-Nafion/IL/SPE is used to improve electrochemical properties, and bismuth is known for its ability to improve sensitivity and selectivity in electrochemical detection processes, particularly for lead [54]. Among the light metals, only aluminum ions (Al^{3+}) were detected in the soil by Square Wave Anodic Stripping Voltammetry (SWASV) through a sensor exploiting the properties of bismuth modified laser induced graphene (LIG) [48]. In [55], a microfluidic impedimetric nitrate sensor using an electrochemical sensing interface enabled by graphene oxide (GO) nanosheets and poly(3,4-ethylenedioxythiophene) nanofibers (PEDOT-NFs) was developed. The sensor has demonstrated the ability to accurately detect and quantify nitrate ions (NO^{3-}) in real samples extracted from soil. The PEDOT NFs-GO composite serves as an effective matrix for immobilization of nitrate reductase (NiR) enzyme molecules. In contrast, in [56], a developed potentiometric LIG electrodes functionalized with a membrane ionophore selective for NH^{4+} or NO^{3-} and used for SC-ISE formation to measure nitrogen in Soil was detected. In [57], nitrate through a hybrid of silver nanoparticles (Ag NPs) and copper(II)-terephthalate metallorganic structures (Cu-BDC MOFs) was detected, which were used as Screen Printed Carbon Electrode (SPCE) modifiers for electrocatalytic nitrate detection.

Table 3 summarizes various sensor types and their performance metrics for detecting heavy metal ions using different techniques. Comparatively analyzing the various electrochemical techniques presented, it can be said that SWASV is a highly sensitive and selective technique for the detection of heavy metals such as Pb(II), Cd(II), and As(III). For example, sensors such as Fe-Chitosan-modified PVC electrodes have demonstrated high sensitivity (6.48 μA/ppb for As(III)) with a very low LOD (1.01 μg/L) in the linear range of 0.02-78 μM and with a stability of 30 days, making them ideal for trace measurements in soil [52]. However, the method can be influenced by environmental conditions and requires careful preparation of the sensor. Stability may vary depending on the modifying material used. Potentiometric techniques offer high selectivity and are particularly useful for detecting specific ions such as Cd(II) and Pb(II). For example, molecular impression polymer (MIP)-based sensors have demonstrated adequate sensitivity with fast response times (14 s) and good stability (up to 10 weeks without significant variations). The sensitivity of these techniques may be lower than voltammetry, and their use is often limited to laboratory conditions rather than in the field. The SWAV technique and the other voltammetric techniques seen offer a detailed analysis of the electrochemical response, making them suitable for complex sensing studies. Modified sensors, such as those with carbon nanotubes or graphene, greatly improve sensitivity and selectivity. They generally require long deposition times (up to 400 s) and interferents, making these techniques more complex to use in practical applications, can affect linearity. Therefore, for heavy metal detection, SWASV remains the preferred technique due to its high sensitivity and low detection limit. Electrodes modified with nanomaterials such as graphene and bismuth nanoparticles are recommended to improve performance under field conditions. Table 4 highlights various sensor types and their analytical performance for detecting herbicides, fungicides, and environmental pollutants like nitrates (NO_3^-) and ammonium (NH_4^+). Techniques such as differential pulse voltammetry (DPV), square wave voltammetry (SWV), cyclic voltammetry (CV), and potentiometric sensing are employed. Sensors, including glassy carbon electrodes (GCE), PVC-based ion-selective electrodes (ASS-ISE), and advanced materials like PEDOT nanofibers with graphene oxide (PEDOT NFs-GO), exhibit excellent sensitivity and low limits of detection (LOD) For the detection of pesticides and herbicides, potentiometric techniques, particularly those using molecularly imprinted polymers, are recommended for the selective detection of specific organic compounds. These sensors offer a good compromise between selectivity, stability, and ease of manufacture. For nitrates, the use of microfluidic impedimetric sensors with graphene oxide nanosheets has shown excellent detection capability. This technique is recommended for fast and accurate measurements in real soil samples as these sensors are highly sensitive, fast and suitable for complex solutions, especially ideal for ported platforms. Despite this, potentiometric sensors (ISE) are cost-effective, simple, and selective for measuring nitrates and other soluble ions in environmental samples such as water and agricultural soils. As an established and widely available technology, they are the preferred choice for such applications.

3.2. *Inline methodologies using near infrared reflectance spectroscopy (NIRS) and laser-induced breakdown spectroscopy (LIBS)*

Inline methodologies, such LIBS and NIRS, offer a promising alternative by providing real-time, on-site analysis of soil properties with minimal sample preparation. This paragraph aims to explore the principles, applications, and benefits of in-line soil analysis methodology using spectroscopy approaches.

LIBS has emerged as a leading technique with significant potential for real-time and large-scale applications [60]. The time-resolved LIBS technique functions by utilizing the avalanche ionization effect triggered by a strong laser beam directed at the sample being studied. The induced plasma usually has temperatures of several eV together with electron densities. This results in the formation of a plasma with temperatures of several eV and electron densities of 1018 electrons/cm^3, respectively [61]. Under these conditions, the material experiences significant ionization and is separated into its atomic parts. This division leads to a powerful light emission as atoms and electrons recombine. The emitted light is then examined to determine the specific emission lines of the elements within the sample. When separating the background generated by the bremsstrahlung continuum from the spectral

Table 3
Performance comparison of electrochemical sensors for detecting heavy metals and light metals.

Sensor type	Detection type	Sensitivity	LOD	Linear range	Stability	Notes	Ref.
PVC SPE with Fe-Chitosan (for As(II))	SWASV	6.48 μA/ppb	1.01 ppb	38.7 to 158.7 μA	10 weeks	Electrochemical detection using chitosan and Fe for As(III)	[52]
SPE (for Cd(II))	SWASV	$y = 0.3221x - 0.1909$	3 μg/L	5.0 to 70.0 μg/L	120 s	Electrochemical detection using IL and graphene for Cd(II)	[58]
SPE (SWCNTs-Nafion/IL/SPE) (for Pb(II))	SWASV	$y = 2.8369x + 2.9025$ (1-10 μg/L), $y = 0.4811x + 27.8450$ (10-100 μg/L)	0.1 μg/L (1-10 μg/L), 0.58 μg/L (10-100 μg/L)	1.0 to 100.0 μg/L	120 s	Composite SPE for Pb(II) detection using SWCNTs and bismuth	[53]
CME-BiFe (for Cd(II), Pb(II))	SWASV	$y = 2.41028x + 4.90492$ (Cd), $y = 0.88737x + 4.41354$ (Pb)	0.1 μg/L (Cd), 0.2 μg/L (Pb)	0 to 50 μg/L	~30 min	Portable system for in situ detection of heavy metals in soil	[59]
Bismuth-modified LIG for Al^{3+}	SWASV	$y = 3.2846x + 160.39$	0.34 ppm (LOD), 1.07 ppm (LOQ)	1.07–300 ppm	Not reported	LIG electrodes modified with bismuth for aluminum ion detection	[45]

Table 4
Performance comparison of electrochemical sensors for detecting organic and inorganic pollutants.

Sensor type	Detection type	Sensitivity	LOD	Linear range	Stability	Notes	Ref
GCE with $GdNbO_4$ (for aclonifen)	DPV	23 μA μM^{-1} cm^{-2}	1.15 nM	0.02–78 μM	30 days	gadolinium niobate ($GdNbO_4$) nanoparticles on the electrode	[51]
PVC ASS-ISE (for Bispyribac Herbicide)	Potentiometric	−47.8 ± 1.1 (r^2 = 0.9995)	1.33 μg/mL (I), 1.81 μg/mL (II)	1.0×10^{-2}–8.6×10^{-6} M (sensor I), 1.0×10^{-2}–9.0×10^{-6} M (sensor II)	Four weeks	MIP (molecularly imprinted polymer) nanospheres embedded in polymer membrane act as receptors for selective bispyribac recognition. PANI film as solid contact.	[43]
PVC ASS-ISE (for dinotefuran) & GCE (for carbendazim)	Potentiometric	Avg. slopes: 66.3 (I), 50.8 (III)	0.35 μg/L (I, III)	10^{-7}–10^{-2} mol L^{-1}	4 weeks (carboxylated PVC sensor 5), 8 weeks (MIPs sensors 1-4)	Dinotefuran sensors using MIPs with acrylamide or methacrylic acid as functional monomer	[50]
GCE (for fungicide)	SWV	Slope: 0.054 (near Nernst)	0.31×10^{-8} M via DPV	Ep(V) = 1.170–0.054 (pH)	20 days	Glassy carbon electrode used for carbendazim detection via electrochemical polymerization	[45]
PEDOT NFs-GO (for NO_3^-)	Potentiometric	61.15 /(mg/L)/cm^2	0.135 mg/L	0.44–442 mg/L	Not reported	NF PEDOT electrospun conjugates GO nanosheets and nitrate reductase (NiR) enzyme as bioelectrode	[55]
SPCE (for NO_3^-)	CV & Amperometric	1159.8 μA mM^{-1} cm^{-2}	0.24 μM	0.5–1000 μM	Two weeks	Silver nanoparticles (Ag NPs) and Cu-BDC MOFs hybrid as SPCE electrode modifiers for nitrate sensing	[57]
LIG SC-ISE (for NH_4^+ & NO_3^-)	Potentiometric	51.7 ± 7.8 mV/dec (NH_4^+), −54.8 ± 2.5 mV/dec (NO_3^-)	28.2 ±25.0 μM (NH_4^+), 20.6 ±14.8 μM (NO_3^-)	10^{-5}–10^{-1} M for both sensors	Low long-term drift of 0.93 mV/h (NH_4^+ sensors) and −5.3 μV/h (NO_3^- sensors)	LIG electrodes functionalized with an ionophoric membrane selective for NH_4^+ or NO_3^-, used to measure nitrogen in soil	[56]

emission of heavy atoms and ions, it is crucial to select the appropriate time delay for the activation of the detection system. [62]. The ability to analyze data in real time is one of the primary benefits of laser-based spectroscopy techniques. In this regard, LIBS enables us to identify several atomic species in a selected spectral area with a single laser pulse. Based on well-known spectra, appropriate algorithms can be created for the real-time data analysis to provide both qualitative and quantitative details on the elemental makeup of the material under investigation. Laser-induced breakdown spectroscopy has been successfully used to determine the content of soil carbon (C) [63,64], [60] macro- and micronutrients [65], [66], [67] and toxic elements [68], [69], [70,71].

Moreover, deep learning-based pollution prediction models using LIBS in soil analysis has emerged as a promising tool for accurate and efficient environmental monitoring. LIBS, an advanced analytical technique, provides rapid, real-time detection of various elements in soil samples, which, when integrated with deep learning algorithms, enables the prediction of soil pollution levels. Recent studies have explored the potential of this combined approach, highlighting its accuracy and applicability. For example, [72] demonstrated how deep learning models, particularly convolutional neural networks (CNNs), could predict heavy metal contamination in soils based on LIBS data. Similarly, a study [73] employed deep neural networks (DNNs) to classify soil contamination levels and predict pollutant concentrations using LIBS spectral data. Another notable work [74] combined LIBS with recurrent neural networks (RNNs) for time-series prediction of soil NOx emission trends. Moreover, [75] applied a hybrid model, integrating LIBS with both machine learning and deep learning techniques to enhance prediction accuracy for various pollutants in agricultural soils.

Table 5
Comparing laser-induced breakdown spectroscopy LIBS and visible near-infrared spectroscopy vis-NIR for predicting soil properties [76] SOC (Soil Organic Caron), RMSEP (Root Mean Square Error of Prediction), RPIQ (Relative Percent Improvement in Quality).

Soil property	LIBS PLSR				Vis-NIR PLSR			
	RMSEP [%]	R^2	RPIQ	BIAS [%]	RMSEP [%]	R^2	RPIQ	BIAS [%]
Clay	5.68	0.62	1.5	−3.52	6.11	0.56	1.4	−3.34
Silt	4.46	0.40	1.6	2.20	4.66	0.34	1.5	3.25
Sand	5.32	0.85	2.7	−1.73	7.71	0.68	1.9	1.14
SOC	0.87	0.67	3.2	−0.04	1.17	0.40	2.4	−0.49

NIRS is a quick, non-invasive, and economical soil analysis technique that eliminates the need for hazardous chemicals. Therefore, NIRS may be highly valuable in soil science for analyzing soil parameters that typically require costly and time-consuming analytical methods. The principle of operation of NIRS for soil analysis involves the interaction of near-infrared light (wavelengths typically ranging from 780 nm to 2500 nm) with soil components. When NIR light is directed onto a soil sample, it is absorbed and reflected by the molecules in the soil. Different molecules absorb and reflect light differently, creating a unique spectral fingerprint for each compound. Some researchers estimate that NIRS can reduce laboratory costs by at least 80% compared to traditional reference methods [77]. Adopting NIRS technology, extensive and geologically uniform soil areas can be thoroughly characterized. In recent years, extensive research has focused on using in-line spectroscopy to detect soil organic matter, nitrogen, phosphorus, and potassium [78–80],[81,82],[83]. Fewer studies on the estimation of heavy metal content are reported in the literature. The partial least squares regression model was utilized in [84] to predict the levels of cadmium and zinc. Additionally, a prediction model has been developed to estimate soil contamination levels of iron, cadmium, copper, lead, nickel, and zinc. [85]. Other examples for detection of Cu, Pb, Zn, Cd, Co, Ni, Fe, Mn and Cr are reported in [86], [87–91].

In Table 5, the performance of LIBS and vis-NIRS was compared based on the prediction accuracy and model performance using Partial Least Squares Regression (PLSR) [76]. A comprehensive dataset of samples from different European countries was utilized to forecast important soil health indicators (soil texture and soil organic carbon). LIBS demonstrated greater accuracy than vis-NIRS in predicting sand, soil organic carbon levels, while both methods showed similar performance in estimating clay content. While the LIBS model performed slightly better than vis-NIRS for predicting silt, both methods exhibited a weak correlation between the measured and predicted silt levels. There was no statistically significant difference between LIBS and vis-NIRS as prediction methods. This study highlights the significant potential of spectroscopic methods, like LIBS and vis-NIRS, for enhancing soil health by enabling quicker and more cost-effective monitoring of essential soil characteristics across a broad geographical area.

4. Inline mapping methods

This chapter aims to describe the electromagnetic compatibility issues that may arise in the underground scenario, as well as the positioning techniques applicable in this challenging environment. The first part of this chapter describes the possible sources of disturbance in the underground scenario, such as scattering obstacles, power grids, high-voltage AC Traction systems, and external sources (i.e., radio transmitters, TV transmitters, and cellular base stations). These elements can affect the measurement accuracy. The paragraph reports the example of several studies that analyzed the effect of electromagnetic disturbances, including those caused by AC/DC electric traction systems, overhead conductors, and lightning-induced disturbances. The main underground positioning techniques are analyzed in the second part of this chapter. In particular, the Ground Penetrating Radar, Radiofrequency, and Magnetic Field localization techniques are described in detail, showing the advantages and limitations of each of them. Due to the comparison between these techniques and the importance of the topic, a section dedicated to magnetic field sensors is reported.

4.1. Electromagnetic compatibility issues in underground scenarios

The measurement of quantities of interest in the underground environments poses several electromagnetic compatibility issues. Indeed, in practical scenarios, the underground environment is characterized by the presence of scattering obstacles (pipes, stones, and metal objects, to cite a few) and electromagnetic interferences due to low-frequency magnetic fields generated by power grids [92] and high-voltage AC Traction systems [93]. Secondary effects are imputable to coupling of the ground grids with external electromagnetic fields generated by radio and TV transmitters and cellular base stations operating nearby. Such interferences can influence the correct operation of the measurement devices and data acquisition systems, thus affecting their measurement accuracy [94]. These aspects have been faced for several years and continuously updated because of the evolution of electrical technologies adopted for modern transportation. As an example, in [95] the transient electromagnetic interference between overhead and underground conductors is analyzed for different soil properties, with the main aim of exploring the effects of HF-induced voltages on underground metallic pipelines due to overhead conductors. The interest in such a topic is confirmed by the recent studies conducted in [96–98], where the effects of electromagnetic interference due to electrical faults of the AC line as well as to specific arrangements and practical case studies are investigated for evaluating the induced voltages on pipeline structures due to such phenomena. In [99] the effects due to lightning-induced disturbances in buried cables are analyzed by considering both model and experimental approaches. In particular, it is shown how significant magnetic and electric field levels can also be experienced hundreds of meters apart from the injection point, whose spectrum is very wide (above 500 MHz), and with currents induced by triggered and natural lightning events both in the buried cable shield and in the inner conductor. In [93,100], the electromagnetic interference due to AC and DC electric traction systems, respectively, were analyzed to evaluate the effects of such kinds of systems in underground environments. In particular, in [93], it was demonstrated that, in some practical circumstances, the harmonics could introduce higher issues than the fundamental frequency, whereas in [100] it is shown how the intensity of radiated electromagnetic fields generated by a DC trolley locomotive system adopted for underground applications appears as significantly higher than typical background noise in the frequency range 250 kHz–3 GHz. All these analyses confirm that underground environments could be generally characterized by several kinds of electromagnetic interference which could affect the correct working of electrical and electronic devices operating in such scenarios.

4.2. Advanced underground positioning techniques

Underground is a challenging environment for localization methods. Indeed, the subsoil does not allow the use of GPS or makes not easy the use of indoor position methods based on vision sensors, wireless sensors, depth sensors, and radio-frequency sensors [37]. This section describes the main localization techniques used in underground environment for different applications like finding buried objects (i.e., pipes or ferromagnetic objects), [10,34,101,102], road and utility monitoring [103], positioning of mobile nodes [9], tracking of the animal movement [104], unexploded ordnance searching [105],

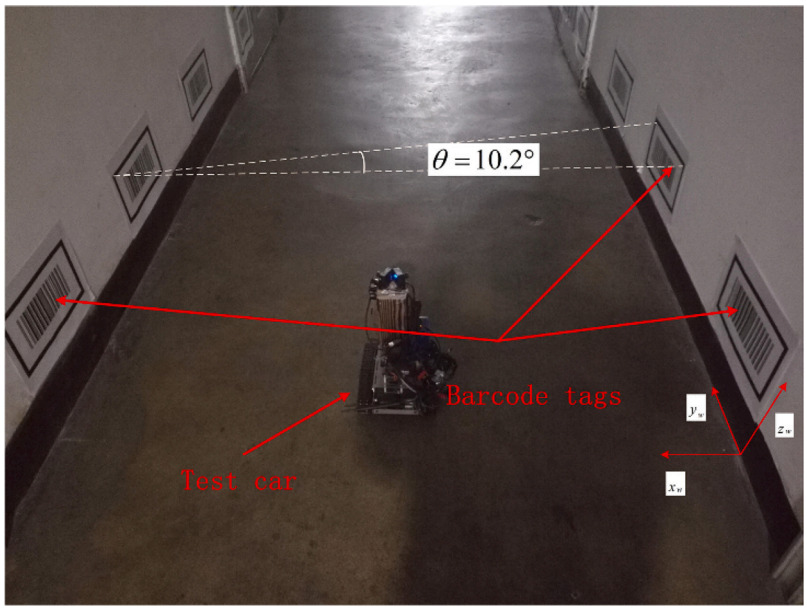

Fig. 3. System proposed in [106] for tracking the position of a vehicle into a mine tunnel. The proposed solution is based on a combination of vision and ultrasound sensors.

and mine tunnel exploration [106,107]. The latter applications see the exploitation of ultrasound sensors in integration with other sensors. For example, in [106] the authors proposed the combination of ultrasonic and electromagnetic signals to estimate the pose of a receiver inside a mine tunnel. Through the trilateration algorithm based on time-to-flight and an ordinary least squares (OLS) estimator, the authors obtain an RMS error typically lower than 70 cm. Another example is represented by Xu et al. in [106] which proposes the combination of ultrasound and vision sensors to track the position of a vehicle inside a mine tunnel (see Fig. 3). The test performed on a tunnel of 4 m width shows an average error on the plane positioning lower than 0.381 m. Instead, in [107] the authors proposed a wireless sensor network based on an ultrasound transmitter attached to the target and an ultrasound receiver placed on the mine tunnel walls. Through the information obtained from the time difference-of-arrival (TDoA) should be possible to estimate the target position even if no data on localization tests are available. On a general note, ultrasounds are widely used in underwater positioning systems [5,6,108] and in bioimaging [7,109,110], as well as in underground scenarios where a tunnel, acting a waveguide, is available [107]. On the other hand, through-soil positioning applications are much less common, due to signal propagation issues, including attenuation and multiple reflection due to the heterogeneity of the soil as a propagation mean. In this regard, through-soil applications of acoustic waves are mostly related to geophysical prospections [111–113]. In particular, in [113] a study of the reflection properties of interfaces between water, oil, and air are discussed. The other mentioned applications see the exploitation of emerging localization techniques like Ground Penetrating Radar, Radiofrequency, and Magnetic Field that are analyzed in detail in the following subsections.

4.2.1. Ground penetrating radar

In recent years, an open challenge in the scientific community has been the exploration and characterization of the subsurface using non-destructive imaging techniques [114]. Due to its flexibility and ease of use, Ground Penetrating Radar (GPR) is becoming one of the leading technologies [8]. Two types of GPR can be found in commercial and experimental equipment, the Pulse-Radar and the Stepped-Frequency Radar. While Pulse Radars emit and receive echoes of the transmitted pulses, Stepped-Frequency Radars split the pulse signal into its spectral components by emitting them sequentially as a series of sinusoidal signals [115]. In GPR systems, frequency bandwidth and spatial and frequency resolution play a fundamental role. Depending on the depth to be investigated, different bandwidths can be defined. In particular, frequencies below 200 MHz can reach depths of 5–7 m; for depths of the order of 3 m, frequencies between 200–700 MHz (radio frequencies) are used; frequencies between 700–3000 MHz can reach depths of around 1 m; and finally, for depths of around 50 cm, higher microwave frequencies are used [8]. Several works in the literature aim to realize and validate GPR systems capable of automatically mapping the subsurface like the one described in [34] that used a mobile robot equipped with a GPR antenna mounted on a specially designed trailer to scan the subsurface. The antenna scans the subsurface by emitting electromagnetic pulses and the collected data are processed to construct a 3D map of the subsurface. To identify salient points corresponding to buried utilities, image processing techniques are then applied to the 2D radargram (B-scan). This system has a considerable size that does not allow it to be an economical and easily usable system even in small spaces. In [103], the authors presented a multi-static GPR for road and utility monitoring applications mounted on small mobile systems. They present several methods to achieve better detection performance of buried objects than the state-of-the-art. The system is characterized by Antipodal Vivaldi Antenna (AVA) elements because they are planar, ultra-wideband (UWB), low cost and easy to manufacture on printed circuit boards. AVA elements have improved the detection of buried objects and reduced the drift between scans. The system's central frequency was 1.5 GHz with a bandwidth of 1.60 GHz. After a validation phase, the system was tested to detect copper and metal objects of different sizes at a depth of 30 cm. Compared to other work, this system utilizes high time bandwidth to reduce peak radio frequency power requirements (26 dBm) and achieve good scan depths while maintaining high field resolution. In addition, it presents a highly digital flexible architecture that supports programmable pulse generation via software and direct RF digitization. Generally, the analysis of the cited works reveals limitations of the GPR system in terms of:

- (i) size, complexity of the measurement setup, and overall system cost;
- (ii) the GPR receiver needs to move over the ground to intercept the return signal echoes generated by underground objects which are in fixed positions.

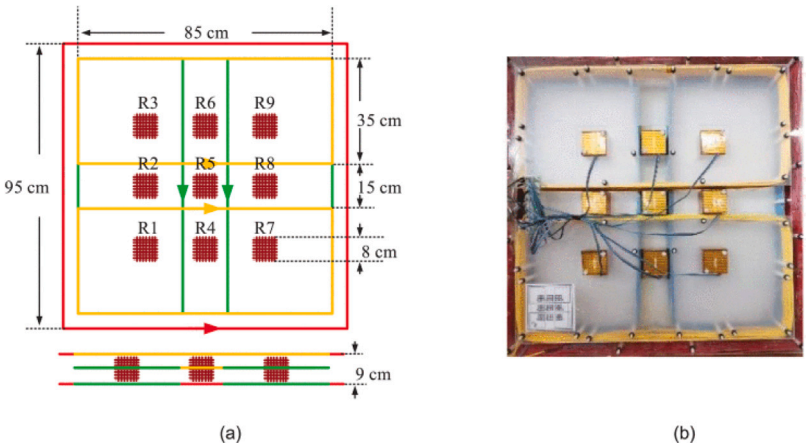

Fig. 4. Array system used in [102] for underground target localization. The system is composed of three orthogonal transmitting coils and an array of nine receiving coils.

4.2.2. Radiofrequency

Systems using Radio Frequency (RF) signals are also used for underground positioning applications, e.g. for the positioning of mobile nodes [9]. Among different RF techniques, there is the Ultra-Wide Band (UWB) system, particularly for underground applications authors in paper [116] designed a large-scale localization UWB wireless sensor network. The experiments to validate the system were conducted in an abandoned air raid shelter with a length of 120 m and a width of 4 m. The results highlighted that the average error obtained for distance estimation is less than 0.3 m. These techniques are not always cost-effective, although they achieve high accuracy in real-world scenarios. In general, UWB devices may require a large number of devices in an underground environment to achieve acceptable coverage and accuracy. Another example of RF technology used for underground applications is ZigBee. In [117] authors propose a comparison between the traditional Received Signal Strength (RSS) technique and Radio Frequency Time-of-Flight (RF-TOF). Experimental tests were carried out in an underground environment and the results show that the distance estimation errors increase according to RSS decrease and the standard deviation of multiple measurements increases with increasing distance. On the contrary, TOF ranging shows excellent performance with minimal standard deviation and the range error does not increase significantly with increasing distance. Most range errors are less than 3 m. However, ZigBee technology is characterized by low data-rate networks, therefore, related applications are limited to low data-rates [9]. WLANs, on the other hand, can provide higher data rates and can receive and transmit information simultaneously, enabling autonomous and remote positioning, but in the underground scenario, this solution may have problems with limited coverage due to the propagation characteristics of the 2.4 and 5 GHz bands [118].

4.2.3. Magnetic fields

Magnetic field-based underground localization is an efficient, low-cost approach used to detect and map underground objects. This method exploits the natural and/or induced magnetic properties of materials to provide information used for accurate and non-invasive localization. Underground localization based on magnetic fields can be classified into two broad approaches: techniques that rely on measuring the deformation of the Earth's magnetic field due to the presence of magnetic anomalies, and techniques that use artificial magnetic fields to stimulate the underground targets and measure their effect. Magnetic Anomaly Detection (MAD) is a powerful and non-invasive tool used to detect and map ferromagnetic objects buried underground. Drones or small ground vehicles are used to scan the area to be investigated; with scalar or vector magnetometers, the magnetic field is detected to create a magnetic map in which it is possible to identify the position and depth of the magnetic anomalies. In [10] the authors present an improved approach to MAD through the development of a new algorithm based on signal modulation. The main goal of the research is to improve the detection capabilities of weak magnetic anomalies, which are often obscured by the geomagnetic background. The authors tested the ability of the algorithm in the detection of a ferromagnetic target having a speed of 4 m/s. They used a linear array of seven magnetic sensors distributed at 15 m from each other. The obtained results showed a good ability to detect anomalies with a low signal-to-noise ratio; in fact, for a weak magnetic anomaly with an SNR of −6.9 dB, the detection probabilities and false alarm rate are approximately 0.9648 and 0.001, respectively. Another methodology for improving results using MAD was proposed in [101]. The paper introduces a new data processing method for magnetic anomaly detection and localization, exploiting two-dimensional orthonormal basis functions (2-D OBFs). The authors tested the proposed method in the detection of an iron pipe buried at 60 cm into the soil using an unmanned aerial vehicle (UAV) with an optically pumped magnetometer. During the measurements, the magnetic sensor was maintained at 1 m above the ground (i.e., the sensor-target distance was approximately 1.6 m). The obtained results showed a localization approaching 0.27 m. The authors reported that with different combinations of pipe size and flight altitudes, the localization error falls in the range 0.1-0.6 m. By applying 2-D OBFs, the method achieves higher localization accuracy and lower false alarm rate than traditional 1-D OBF methods. The 2-D approach effectively handles multiple targets and overlapping anomalies, a common challenge in MAD applications. An interesting application using magnetic field anomalies is presented in [37], where a resilient method for underground localization is proposed to improve the accuracy of directional drilling. The main innovation of this method is the ability to use only the magnetic field distribution of each region, obtained via two vector magnetometers, to detect constraints between poses by comparing magnetic field sequences. This is particularly effective in the underground environment where the soil composition varies; causing distinct magnetic field anomalies that can be remeasured due to the repetitive forward and backward motion of the drilling system. The authors tested the proposed method in the detection of a directional drilling system inside nine concrete blocks. The obtained results showed a RMSE on the translation and on the orientation equal to 0.038 m and 0.326°, respectively. Underground localization using artificial magnetic fields involves the generation and measurement of magnetic fields to identify and localize objects beneath the surface. This approach typically uses magnetic field transmitters to create a controlled magnetic environment and sensor receivers to measure the response, facilitating the accurate localization of underground objects. Typically, coils that generate magnetic fields with frequencies not exceeding about 10 MHz are used as transmitters, while the receiving part is made using magnetometers capable of measuring alternating

Table 6
Summary of the mentioned positioning techniques with respect to the technology used, the application field, the domain size, and the obtained performances. RMSE: Root Mean Square Error; AE: Average Error. DBO: Detection of Buried Object. MTE: mine tunnel exploration. RUM: Road and utility monitoring. RTP: Real-time position estimation of personnel in harsh environment. DDS: Detection of a directional drilling system. TAM: Tracking of animal movement. UOD: Unexploded ordnance detection.

Technology	Ref.	Application	Domain size	Obtained performance
Ultrasound + e. m. signals	[9]	MTE	2D, N/A	RMSE < 0.70 m
Ultrasound + vision sensors	[106]	MTE	2D, horseshoe-shaped tunnel, width 4 m	AE < 0.381 m
GPR	[34]	DBO	2D, N/A	N/A
	[103]	RUM	2D, N/A	N/A
Radio-frequency	[116]	MTE	2D, 120 m × 4 m	AE < 0.3 m
	[117]	RTP	2D, N/A	AE < 3 m
Magnetic anomaly detection	[10]	DBO	2D, 90 m × 50 m	N/A
	[101]	DBO	2D, 20 m × 20 m	RMSE 0.27 m
	[37]	DDS	3D, 9 m × 1 m × 1 m	$RMSE_{translation}$ 0.038 m $RMSE_{orientation}$ 0.326°
Artificial magnetic field	[104]	TAM	2D, 15 m × 15 m	RMSE 0.45 m
	[105]	UOD	2D, 0.5 m × 0.5 m	AE 0.04 m
	[102]	DBO	3D, 13 m × 8 m × 2 m	AE 0.10 m

magnetic fields [119,120]. In [104] the authors present a system for 3D underground localization of animals, using magneto-inductive (MI) tracking. The proposed system takes advantage of low-frequency magnetic fields, which can penetrate the ground with minimal loss, to achieve accurate localization. The system uses an array of transmitting coils located above the area of interest, which generate magnetic fields at a frequency of 125 kHz in time division, and three orthogonal receiving coils, placed in a collar attached to the animals, for measuring the magnetic field. The localization system achieved a typical accuracy of 0.45 m RMS over an investigation area of 15 m × 15 m. An interesting approach to avoid introducing sensors underground is the one presented in [102,105]. These papers discuss a method for underground target localization using a magnetic gradient tensor approach combined with a towed transient electromagnetic sensor array. To carry out the underground investigation, the entire system (transmitting and receiving coils) is moved using a small handling system similar to the analysis carried out using GPR. In [105] the authors present an advanced method for rapid localization of underground targets using a magnetic gradient tensor combined with the Gauss–Newton algorithm. Through the proposed methodology, both horizontal and depth localization errors of less than 4 cm were obtained. Furthermore, in [102] the authors present a novel method for underground target localization using an improved magnetic gradient tensor approach. The system consists of three orthogonal transmitting coils and an array of nine receiving coils, all above ground, designed to operate in both survey and cued modes (see Fig. 4). In survey mode, the *z*-axis transmitting coil generates a 125 Hz magnetic field to roughly estimate target positions. In cued mode, the three transmitter coils sequentially generate magnetic fields at 12.5 Hz. The system uses the different responses to better estimate target positions and distinguish between multiple overlapping targets. This dual-response approach improves localization accuracy for both shallow and deep targets. The obtained results demonstrated the effectiveness of the proposed method, ensuring both depth and horizontal errors of no more than 10 cm each, for targets placed up to 2 meters deep. Table 6 shows a comparison of the mentioned positioning techniques with respect to the technology used, the application field, the domain size, and the obtained performances. Due to the importance of the topic, the following section is specifically devoted to magnetic field sensors.

4.3. Magnetic field sensors

Magnetic field sensing is a good candidate for positioning purposes, since the magnetic field can penetrate most known materials. As such, it is already used in indoor positioning scenarios or in accurate short-range positioning [123–127]. Several magnetic field sensors are available that introduce different compromises between accuracy, cost, suitability for embedded systems and for specific applications. The sensor resolution is an important parameter, since it defines the achievable performance of ranging and positioning systems. For instance, since the geomagnetic field intensity is in the range of 25 to 65 μT, sensors with a worse accuracy would not be able to detect local field variations, Similarly, if an artificial magnetic field is introduced either by known position anchors or by a mobile node, the sensor resolution will define the system range. Fig. 5 was obtained by assuming a planar coil with a diameter of 50 cm, fed by a 1 A current at a frequency of 500 Hz and placed at a height of 1 m with respect to the ground, that is the coil center has coordinates [0 0 1 m]. Using a magnetic dipole based model the B field generated at a depth of 1 m for increasing distances with respect to the coil was obtained. Fig. 5 also shows the resolution of commercial sensors based on different technologies, associating their resolution with the achievable operational range. The main sensing technologies include induction coils, Hall Effect (HE) sensors, Magneto-Resistive (MR), that include

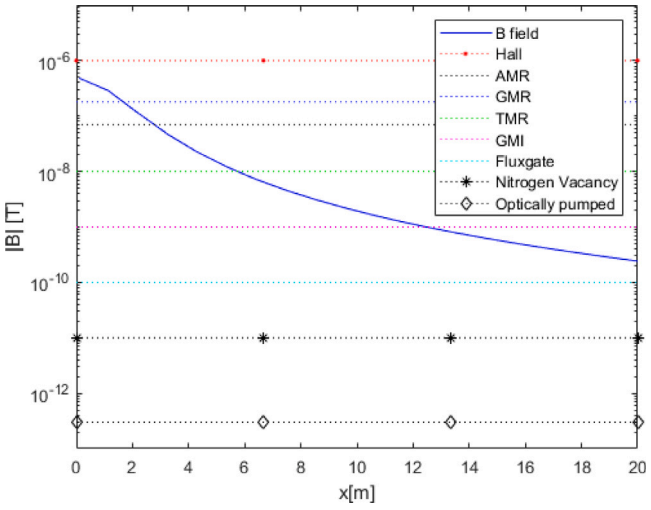

Fig. 5. B field intensity for a coil with 100 windings and a diameter of 50 cm, fed by a current of 1 A, placed at 1 m above the ground. The B field is obtained at a depth of 1 m. The horizontal lines show the resolution of some families of magnetic field sensors, obtained from datasheets of commercial products.

Table 7
Performance metrics for main commercial magnetic field sensors. The performance metrics were expressed in the same measurement units, assuming a unitary magnetic permittivity for parameters expressed in Oersted in the datasheets. Resolution was expressed in bits for sensors with digital output. Accuracy was omitted for TMS sensors, since the commercial devices are designed for angular measurements, and the magnetic field accuracy is not explicitly stated. Optical fiber for magnetic field sensing was proposed very recently and commercial devices are not currently available. The sensitivity was nevertheless included for the sake of completeness.

Type	Temperature	Sensitivity	Resolution	Range	Bandwidth	Accuracy	Noise	Power
Hall	−40 °C–125 °C	1%/μT	1 μT, 12–16 bit	0.2-266 mT	3.5 kHz–5 MHz	1%	9 μT–350 μT rms	27 mW
AMR	−40 °C–150 °C	0.001%/μT	70 nT, 16 bit	6 μT–600 μT	100 kHz–5 MHz	1%	30 nV–500 μV rms	50 mW
GMR	−50 °C–125 °C	0.12%/μT	0.18 μT, 12–16 bit	10 μT–50 mT	100 kHz–1 MHz	0.1%	8 mA rms 1 MHz	50 mW
TMR	−40 °C–150 °C	0.004–0.007%/μT	10 nT, 12–18 bit	6 mT–120 mT	5 kHz	–	700 nV rms/$\sqrt{\text{Hz}}$ 1 Hz	72 μW
GMI	−40 °C–85 °C	8.3%-250%/μT	1 nT–12 μT, 12 bit	0.7 μT–50 mT	4.9 kHz–1 MHz	0.6%	1.5 mV rms	6 mW
Fluxgate	−40 °C–85 °C	1 V/μT	10–100 pT	2–200 μT	3 kHz	0.5%	6 pT rms/$\sqrt{\text{Hz}}$ 1 Hz	400 mW
Optical fiber	– –	2 pm/mT–5 nm/mT (wavelength/induction field)	– –	– –	– –	– –	– –	– –
Optically pumped	−15 °C–55 °C	– –	QTFM [121]: 300 fT QZFM [122]: 20 fT	1–150 μT ±5 nT	500 Hz 3–100 Hz	– –	3 pT/$\sqrt{\text{Hz}}$ 7–10 fT/$\sqrt{\text{Hz}}$	3.5 W 5 W
N–Vacancy	room temp.	–	10 pT	±1.5–±500 μT	200–1000 Hz		10 pT/$\sqrt{\text{Hz}}$	10 W

as sub-classes the Anisotropic Magnetoresistance (AMR), Tunnel Magnetoresistance (TMR), Giant Magnetoresistance (GMR), Giant Magneto Impedance (GMI) sensors, the Superconducting Quantum Interference Devices (SQUIDs), Fluxgate sensors and Optical Fiber (OF) sensors. With exception of SQUIDs, which are unsuitable for the considered application due to high costs and the need for cryogenic temperature, each of them is discussed in the following subsections. All of them are briefly described in the following, while the characteristics of the main off-the-shelves sensors are summarized in Table 7.

Induction coils. Induction coils generate voltage through changing magnetic flux, as described by Faraday–Neumann–Lenz law [128]. They are highly sensitive but limited to detecting AC fields. Miniaturization is challenging due to reduced sensitivity in smaller coils. Using resonant coils with tuned capacitors improves performance by increasing the Q factor [129].

Hall sensors. Hall sensors rely on the Lorentz force, offering simple, low-cost designs with good linearity, scalability, and CMOS integration [128,130]. Recent advancements include the Anomalous Hall Effect (AHE) and Quantum Anomalous Hall Effect (QAHE). Drawbacks include weak output signals, temperature-dependent drift, and offset issues, addressed by conditioning circuits in commercial sensors.

Magneto-resistive (MR) sensors. MR sensors detect magnetic fields through resistance changes in materials. Variants include AMR, GMR, and TMR sensors. A typical performance metric for such sensors is the MR ratio, defined as the change of the resistance of the considered material when exposed to an external magnetic field. For anisotropic materials MR ratio is often defined with respect to two resistance values, obtained for magnetizations respectively orthogonal and parallel to the current [131].

AMR sensors. Anisotropic Magneto Resistance (AMR), discovered in 1857 by Thomson, arises from spin–orbit interaction [132,133]. It manifests as reduced resistance with increasing magnetic field. AMR sensors are primarily sensitive to magnetic fields orthogonal to the sensing element, [131,134]. AMR sensors are used for magnetic field direction detection and 2D encoders, employing a Wheatstone bridge and A/D converters [132,133]. They feature better SNR at low frequencies than GMR or TMR sensors but have lower sensitivity, with a typical MR ratio of a few percent [135].

GMR sensors. Discovered in 1988 by Fert and Grünberg (Nobel Prize, 2007), GMR sensors consist of two ferromagnetic layers separated by a conductive layer. One layer's magnetization is fixed, while the other depends on the external magnetic field. The resistance is related to θ_p and θ_f that are the magnetization angles of the reference and free layers, respectively [131,136]. GMR sensors achieve MR ratios exceeding 50% and are ideal for angle and magnetic field measurements [136,137] relying on Wheatstone bridges [138]. They offer higher sensitivity (100×AMR sensors), making them suitable for applications like hard drive heads, tactile sensors, position sensing (resolution: 2.5 nm), and industrial current sensors [139,140].

TMR sensors. Tunnel Magnetoresistance (TMR) sensors feature magnetic tunnel junctions (MTJs) with ferromagnetic–insulator–ferromagnetic layers. A thin insulating layer enables electron tunneling, enhancing sensitivity up to 300% [131,136]. TMR sensors minimize resistance when magnetizations are parallel and outperform equivalent AMR sensors with twice the sensitivity, 200×lower power consumption, and a 5×wider field range [141]. They are widely used for contactless current sensing and high-sensitivity magnetic field detection [140,142].

GMI sensors. The Giant Magneto Impedance (GMI) effect involves large impedance changes in a ferromagnetic wire carrying AC current when exposed to a magnetic field [131,143]. The skin depth (δ) depends on the frequency (f), conductivity (σ), and permeability (μ). [144]. The impedance varies as a nonlinear function of the magnetic field (HeH_e), with an MR ratio up to 800% [145,146]. GMI sensors, often using AC bridges, are promising for high-resolution applications (down to 1 nT) [146,147].

Fluxgate sensors. Fluxgate sensors use a soft magnetic core magnetized to saturation by an AC current in a solenoid. External magnetic fields disrupt symmetrical saturation, causing transient flux variations detectable by a secondary coil [129,148]. These sensors provide high accuracy and low noise, with sensitivity close to SQUIDs but operable at room temperature [149]. While bulky and power-intensive, recent developments include miniaturization using CMOS, MEMS, and microprinting techniques [150,151]. They are used in geomagnetic field measurement and automotive current sensing, with typical sensitivity of 0.1 V/μT and noise levels of 6–20 pT/$\sqrt{\text{Hz}}$ [152,153].

FO sensors. Fiber optic (FO) magnetic sensors are immune to electromagnetic interference and suitable for harsh environments like gas pipelines [154,155]. Tapered optical fibers (TOFs) have a sensing region where an evanescent field interacts with external magnetic materials, such as magnetic fluids, affecting the refractive index [154,156]. FO sensors achieve sensitivities ranging from 2 pm/mT to 5 nm/mT, offering a safe, corrosion-resistant, and non-invasive magnetic sensing solution [154,157].

Optically-pumped magnetometers. Optically-Pumped magnetometers are highly sensitive quantum sensors that measure extremely weak magnetic fields without requiring cryogenic cooling [158,159]. They use vapors of alkali metals, such as cesium, rubidium or potassium, contained in a glass cell. A laser optically pumps the atoms, aligning the spins of their outer electrons. When exposed to an external magnetic field, spin precesses at a frequency proportional to the field strength (Larmor precession). Depending on the phase of the precession, the atoms absorb light differently, making the atomic vapor more or less

transparent to the laser light. The change in atomic transparency is detected by a photodiode, enabling precise magnetic field measurements. Optically-Pumped Magnetometers can achieve 1 fT resolution. Commercially available instruments can achieve a resolution of 100 fT in a band of about 100 HZ, with a noise floor that depends on the configuration, typically 7-10 fT/$\sqrt{\text{Hz}}$, 15 fT/$\sqrt{\text{Hz}}$, 3 pT/$\sqrt{\text{Hz}}$, 0.1 nT/$\sqrt{\text{Hz}}$ [121,122], with bandwidth from 3–100 Hz up to 500 Hz.

Nitrogen-vacancy magnetometers. The physical principle of Nitrogen-Vacancy Magnetometers is analogous to that of Optically-Pumped Magnetometers, point defects in semiconductor crystals (typically diamond) playing the same role as the atomic vapor [160]. A nitrogen-vacancy center is a point defect in the diamond lattice where a carbon atom is replaced by a nitrogen atom, and an adjacent carbon site remains vacant. This defect introduces localized electronic states within the band gap of diamond. In the presence of a magnetic field, the energy levels of the nitrogen-vacancy spin states shift due to the Zeeman effect. This shift can be detected using optically detected magnetic resonance (ODMR): by applying microwaves and scanning their frequency, one can determine the nitrogen-vacancy resonance frequency, which encodes the local magnetic field. Nitrogen-Vacancy Magnetometers can achieve 1–10 pT resolution. Commercially available instruments achieve a noise floor of 10 pT/$\sqrt{\text{Hz}}$, with bandwidth 200 Hz, extendable up to kHz regime [161].

5. Discussion and conclusions

The paper delves into the critical need for timely and accurate monitoring of soil contamination, an issue with profound implications for environmental protection, disaster management, and decision-making. It highlights the causes, impacts, and advancements in technology that aim to improve our ability to analyze and mitigate soil pollution. Additionally, it presents an in-depth review of robotic systems designed for underground exploration, showcasing their potential for several applications ranging from environmental monitoring to planetary exploration. The paper explores several aspects such as soil contamination challenges, emerging monitoring techniques, and the capabilities and limitations of modern autonomous robotic systems.

Soil contamination arises primarily from anthropogenic activities such as industrial emissions, agricultural runoff, and waste disposal. The accumulation of pollutants—whether organic (e.g., pesticides and industrial solvents) or inorganic (e.g., heavy metals and nitrates)—compromises soil's functionality, threatening ecosystems, groundwater, and human health. Addressing contamination requires a robust understanding of pollutant sources, distribution, and concentration. Traditional laboratory-based methods, such as spectroscopy and mass spectrometry, are reliable but slow, expensive, and limited in spatial coverage. Moving towards real-time, in-line monitoring systems represents a paradigm shift. Technologies like near-infrared (NIR) spectroscopy and electrochemical sensors provide immediate feedback on soil health, enabling proactive interventions. For instance, electrochemical sensors can detect heavy metals and organic pollutants with high sensitivity, while spectroscopy methods like NIR and Laser-Induced Breakdown Spectroscopy (LIBS) offer non-invasive, large-scale analysis capabilities. These innovations are essential for precision agriculture and environmental remediation, as they balance accuracy, efficiency, and scalability.

Incorporating real-time sensing technologies, such as electrochemical sensors and spectroscopy-based techniques like LIBS and NIRS, offers promising prospects for cost-effective, spatially resolved soil monitoring. For example, electrochemical sensors, using Square Wave Anodic Stripping Voltammetry (SWASV), demonstrated detection capabilities with Fe-Chitosan-modified PVC electrodes achieving a sensitivity of 6.48 μA/ppb for As(III), with a detection limit (LOD) of 1.01 μg/L. Spectroscopic methods such as LIBS, with plasma emissions reaching temperatures of several eV, have improved soil pollution prediction accuracy when integrated with deep learning models. Notably, NIRS has demonstrated its ability to reduce laboratory costs by at least 80% compared to conventional methods, offering rapid, chemical-free alternatives for soil diagnostics. Furthermore, Near-Infrared Reflectance Spectroscopy (NIRS) and Laser-Induced Breakdown Spectroscopy (LIBS) can benefit from AI and machine learning. These emerging technologies can enhance predictive modeling, automate soil classification, and improve the accuracy of spectroscopic techniques. Regarding electrochemical sensors, an interesting approach reported in the literature is the adoption of nanomaterials like carbon nanotubes, graphene, and metal oxide nanoparticles, which seem to enhance sensitivity in detecting heavy metals, nitrates, and organic pollutants. New polymer-based nanostructures also show promise in enhancing sensitivity for detecting pesticides. The integration of electrochemical sensors with nanomaterials is becoming increasingly cost-effective due to advancements in miniaturization and mass production. However, challenges remain in large-scale deployment, including sensor calibration and long-term stability. Several commercial electrochemical sensor systems are already available for soil monitoring, such as PalmSens, which offers a portable electrochemical solution for field-based heavy metal and organic pollutants analysis.

In autonomous soil monitoring solutions, unmanned vehicles, including drones and robotic systems, play a significant role. These devices can access hazardous or hard-to-reach areas, providing real-time data on shallow soil contamination. For example, drones equipped with advanced sensors can map pollutant distribution, ensuring reliable data collection for targeted clean-up efforts. However, challenges such as limited underground positioning and electromagnetic interference remain significant hurdles to widespread adoption. Recent developments in underground robotic systems, such as the DIGBOT and Mole-Bot, highlight substantial progress. The DIGBOT achieved a penetration rate of 114 mm/min in polypropylene pellets, demonstrating efficient drilling performance without a full locomotion module. The Mole-Bot, capable of drilling holes up to 202 mm in expanded configurations, integrated 3D SLAM localization, achieving a positional error of only 0.13 m over a 5-meter distance, underscoring its potential for autonomous underground navigation. Despite their potential, many robots still lack integrated soil analysis capabilities, limiting their utility in contamination monitoring. The BADGER robot, while offering one of the most complete motion and navigation architectures, faces challenges due to its energy consumption of 7–8 kW, posing obstacles for field deployment.

Underground positioning systems have also seen advancements. For instance, magnetic anomaly detection (MAD) for an iron pipe at 60 cm depth achieved localization accuracy of approximately 0.27 m, and experiments with Radio Frequency (RF) systems, particularly Ultra-Wideband (UWB), demonstrated distance estimation errors of less than 0.3 m. To this aim magnetic sensors are also a viable solution, since with the exception of Fluxgates they can be realized as embedded devices with a low power consumption not exceeding 50 mW and small space occupation in the range of a few cm^3, already available on the market. Consequently, they can easily be included in a small drilling robot with low risk of violating mass, volume, or power constraints, realizing a positioning system based on active anchors. It is also worth noting that cheapest sensors, like the Hall ones, are less performing in terms of B-field resolution which is about 1 μ T, reducing the operational range (see Fig. 5). If budget constraints prevent the use of expensive high performance sensors, a potential solution is increasing the generated B-field, since active anchors are not subject to same constraints affecting the design of the drilling robot. These results highlight significant improvements in the accuracy and reliability of underground localization techniques, offering robust solutions for mapping and monitoring underground contamination sites.

The combination of these emerging technologies—including electrochemical sensors, spectroscopy, and advanced robotic systems—presents a holistic approach to soil health monitoring. While challenges such as sensor calibration, large-scale deployment, and environmental

interference remain, advancements in these fields will significantly enhance precision agriculture, environmental sustainability, disaster preparedness, and resource management. For instance, inline techniques represent greater efficiency, reducing the time and costs associated with traditional soil sampling methods, and offering the ability to identify contamination locations and types more rapidly.

In conclusion, the paper underscores the importance of technological innovation in addressing soil contamination and advancing underground exploration. Real-time, in-line monitoring systems and robotic technologies represent significant strides towards efficient, scalable solutions for environmental management. However, ongoing research and development are needed to overcome current limitations, ensuring these tools meet the growing demands of precision agriculture, disaster mitigation, and planetary exploration. With sustained focus and collaboration, these technologies have the potential to transform our approach to soil health and environmental stewardship.

CRediT authorship contribution statement

Valerio Brunacci: Writing – original draft, Visualization, Validation, Investigation, Data curation. **Domenico Capriglione:** Writing – review & editing, Writing – original draft, Supervision, Project administration, Methodology, Investigation, Funding acquisition, Conceptualization. **Chiara Carissimo:** Writing – original draft, Visualization, Validation, Methodology, Formal analysis, Data curation. **Damiano Crescini:** Writing – review & editing, Writing – original draft, Validation, Formal analysis, Conceptualization. **Filippo Milano:** Writing – review & editing, Writing – original draft, Visualization, Methodology, Formal analysis, Conceptualization. **Nicola Moggia:** Writing – original draft, Visualization, Formal analysis, Data curation. **Antonio Moschitta:** Writing – review & editing, Writing – original draft, Supervision, Resources, Investigation, Funding acquisition, Formal analysis, Conceptualization. **Giorgia Polidori:** Writing – review & editing, Writing – original draft, Data curation. **Cecilia Provenzale:** Writing – original draft, Visualization, Resources, Investigation, Data curation. **Francesco Santoni:** Writing – review & editing, Writing – original draft, Visualization, Methodology, Data curation. **Emilio Sardini:** Writing – review & editing, Supervision, Project administration, Funding acquisition, Formal analysis, Conceptualization. **Mauro Serpelloni:** Writing – review & editing, Validation, Supervision, Project administration, Methodology, Conceptualization.

Declaration of competing interest

The authors declare that they have no known competing financial interests or personal relationships that could have appeared to influence the work reported in this paper.

Acknowledgments

This research activity was funded by the European Union (NextGenerationEU) and by the Italian MUR (Ministry of University and Research) through PRIN PROJECT “New sensors and measurement techniques for underground monitoring and mapping”, Project number 2022P3JY7N, Project CUP D53D23001390006, whose support the Authors gratefully acknowledge.

Data availability

Data will be made available on request.

References

[1] G. Polidori, S. Tonello, M. Serpelloni, Ion-selective all-solid-state printed sensors: A systematic review, IEEE Sensors J. 24 (6) (2024) 7375–7394, http://dx.doi.org/10.1109/JSEN.2024.3354321.

[2] F. Criscuolo, M.I.N. Hanitra, I. Taurino, S. Carrara, G. De Micheli, All-solid-state ion-selective electrodes: A tutorial for correct practice, IEEE Sensors J. 21 (20) (2021) 22143–22154, http://dx.doi.org/10.1109/JSEN.2021.3099209.

[3] A.A. Jennings, Analysis of worldwide regulatory guidance values for the most commonly regulated elemental surface soil contamination, J. Environ. Manag. 118 (2013) 72–95, http://dx.doi.org/10.1016/j.jenvman.2012.12.032.

[4] F. Ramón, C. Lull, Legal measures to prevent and manage soil contamination and to increase food safety for consumer health: The case of Spain, Environ. Pollut. 250 (2019) 883–891, http://dx.doi.org/10.1016/j.envpol.2019.04.074.

[5] D.J. Schott, M. Faisal, F. Hoeflinger, L.M. Reindl, J.B. Andreú, C. Schindelhauer, Underwater localization utilizing a modified acoustic indoor tracking system, in: 2017 IEEE 7th International Conference on Underwater System Technology: Theory and Applications, USYS, 2017, pp. 1–5, http://dx.doi.org/10.1109/USYS.2017.8309451.

[6] E.P. Rodrigues, F. Buiochi, Development of a 500 kHz pulse-echo acquisition system for three-dimensional ultrasound images of objects immersed in water, in: 2023 15th IEEE International Conference on Industry Applications, INDUSCON, 2023, pp. 1631–1636, http://dx.doi.org/10.1109/INDUSCON58041.2023.10374916.

[7] C. Baker, D. Sarno, R.J. Eckersley, B. Zeqiri, Ring artifact correction for phase-insensitive ultrasound computed tomography, IEEE Trans. Ultrason. Ferroelectr. Freq. Control 67 (3) (2020) 513–525, http://dx.doi.org/10.1109/TUFFC.2019.2948429.

[8] M. Ambrosanio, M.T. Bevacqua, T. Isernia, V. Pascazio, The tomographic approach to ground-penetrating radar for underground exploration and monitoring: A more user-friendly and unconventional method for subsurface investigation, IEEE Signal Process. Mag. 36 (4) (2019) 62–73, http://dx.doi.org/10.1109/MSP.2019.2909433.

[9] F. Seguel, P. Palacios-Játiva, C.A. Azurdia-Meza, N. Krommenacker, P. Charpentier, I. Soto, Underground mine positioning: A review, IEEE Sensors J. 22 (6) (2022) 4755–4771, http://dx.doi.org/10.1109/JSEN.2021.3112547.

[10] L. Chen, Y. Feng, P. Wu, W. Zhu, G. Fang, An innovative magnetic anomaly detection algorithm based on signal modulation, IEEE Trans. Magn. 56 (9) (2020) 1–9, http://dx.doi.org/10.1109/TMAG.2020.3005896.

[11] J. Kim, H.W. Jang, J.-U. Shin, J.-W. Hong, H. Myung, Development of a mole-like drilling robot system for shallow drilling, IEEE Access 6 (2018) 76454–76463, http://dx.doi.org/10.1109/ACCESS.2018.2884495.

[12] J. Lee, C. Tirtawardhana, H.W. Jang, J.-W. Hong, H. Myung, Concept design of a novel bio-inspired drilling system for shallow drilling, in: 2019 19th International Conference on Control, Automation and Systems, ICCAS, 2019, pp. 1276–1280, http://dx.doi.org/10.23919/ICCAS47443.2019.8971518.

[13] J. Lee, C. Tirtawardhana, H. Myung, Development and analysis of digging and soil removing mechanisms for mole-bot: Bio-inspired mole-like drilling robot, in: 2020 IEEE/RSJ International Conference on Intelligent Robots and Systems, IROS, 2020, pp. 7792–7799, http://dx.doi.org/10.1109/IROS45743.2020.9341230.

[14] A. Sadeghi, A. Tonazzini, L. Popova, B. Mazzolai, A novel growing device inspired by plant root soil penetration behaviors, PLoS One 9 (2) (2014) http://dx.doi.org/10.1371/journal.pone.0090139.

[15] B. Mazzolai, A. Mondini, P. Corradi, C. Laschi, V. Mattoli, E. Sinibaldi, P. Dario, A miniaturized mechatronic system inspired by plant roots for soil exploration, IEEE/ASME Trans. Mechatronics 16 (2) (2011) 201–212, http://dx.doi.org/10.1109/TMECH.2009.2038997.

[16] Y. Gu, H. Date, Y. Kawamura, Underground locomotion by snake-like robot, Proc. JSME Annu. Conf. Robot. Mechatronics (Robomec) 2018 (2018) 2P1–E09, http://dx.doi.org/10.1299/jsmermd.2018.2P1-E09.

[17] R. Abe, Y. Kawamura, K. Kamijima, K. Murakami, Performance evaluation of contra-rotating drill for DIGBOT, in: Proceedings of SICE Annual Conference 2010, 2010, pp. 885–888.

[18] P. Vartholomeos, P. Marantos, G. Karras, E. Menendez, M. Rodriguez, S. Martinez, C. Balaguer, Modeling, gait sequence design, and control architecture of BADGER underground robot, IEEE Robot. Autom. Lett. 6 (2) (2021) 1160–1167, http://dx.doi.org/10.1109/LRA.2021.3056068.

[19] K. Worrall, C. Houston, M. Cebecauer, T. Flessa, E. Mcgookin, D. Thomson, P. Harkness, Design and implementation of a control system for a tunneling robot, in: 2019 IEEE SmartWorld, Ubiquitous Intelligence & Computing, Advanced & Trusted Computing, Scalable Computing & Communications, Cloud & Big Data Computing, Internet of People and Smart City Innovation, SmartWorld/SCALCOM/UIC/ATC/CBDCom/IOP/SCI, 2019, pp. 242–247, http://dx.doi.org/10.1109/SmartWorld-UIC-ATC-SCALCOM-IOP-SCI.2019.00084.

[20] T. Kubota, H. Omori, T. Murakami, H. Nagai, T. Nakamura, Subsurface explorer robot with peristaltic crawling mechanism, in: Earth and Space 2012: Engineering, Science, Construction, and Operations in Challenging Environments, ASCE, 2012, pp. 583–591, http://dx.doi.org/10.1061/9780784412190.0.

[21] H. Omori, T. Murakami, H. Nagai, T. Nakamura, T. Kubota, Planetary subsurface explorer robot with propulsion units for peristaltic crawling, in: 2011 IEEE International Conference on Robotics and Automation, 2011, pp. 649–654, http://dx.doi.org/10.1109/ICRA.2011.5979824.

[22] H. Omori, T. Murakami, H. Nagai, T. Nakamura, T. Kubota, Validation of the measuring condition for a planetary subsurface explorer robot that uses peristaltic crawling, in: 2013 IEEE Aerospace Conference, 2013, pp. 1–9, http://dx.doi.org/10.1109/AERO.2013.6496960.

[23] W. Zhang, S. Jiang, D. Tang, H. Chen, J. Liang, Drilling load model of an inchworm boring robot for lunar subsurface exploration, Int. J. Aerosp. Eng. 2017 (1) (2017) 1282791, http://dx.doi.org/10.1155/2017/1282791.

[24] W. Zhang, L. Li, S. Jiang, J. Ji, Z. Deng, Inchworm drilling system for planetary subsurface exploration, IEEE/ASME Trans. Mechatronics 25 (2) (2020) 837–847, http://dx.doi.org/10.1109/TMECH.2019.2962500.

[25] T. Dewei, Z. Weiwei, J. Shengyuan, S. Yi, C. Huazhi, Development of an inchworm boring robot(IBR) for planetary subsurface exploration, in: 2015 IEEE International Conference on Robotics and Biomimetics, ROBIO, 2015, pp. 2109–2114, http://dx.doi.org/10.1109/ROBIO.2015.7419085.

[26] W. Zhang, S. Jiang, Y. Shen, P. Li, H. Chen, Development of an inchworm-type drilling test-bed for planetary subsurface exploration and preliminary experiments, in: 2016 IEEE International Conference on Robotics and Biomimetics, ROBIO, 2016, pp. 2187–2191, http://dx.doi.org/10.1109/ROBIO.2016.7866654.

[27] H. Omori, T. Murakami, H. Nagai, T. Nakamura, T. Kubota, Development of a novel bio-inspired planetary subsurface explorer: Initial experimental study by prototype excavator with propulsion and excavation units, IEEE/ASME Trans. Mechatronics 18 (2) (2013) 459–470, http://dx.doi.org/10.1109/TMECH.2012.2222429.

[28] C.R. Stoker, et al., The mars underground mole (MUM): A subsurface penetration device with infrared reflectance and Raman spectroscopic sensing capability, 2003, https://ntrs.nasa.gov/citations/20030111523.

[29] F. Becker, S. Boerner, R. Lichtenheldt, K. Zimmermann, Enabling autonomous locomotion into sand - A mobile and modular drilling robot, in: Proceedings of ISR 2016: 47st International Symposium on Robotics, 2016, pp. 1–6.

[30] R. Lichtenheldt, F. Becker, K. Zimmermann, Screw-driven robot for locomotion into sand, in: Engineering for a Changing World: Proceedings; 59th IWK, Ilmenau Scientific Colloquium, Technische Universität Ilmenau, September 11-15, 2017 59, no. 3.1.06, Ilmenau, 2017, URL https://www.db-thueringen.de/receive/dbt_mods_00033176.

[31] C. Darukhanavala, A. Lycas, A. Mittal, A. Suresh, Design of a bimodal self-burying robot, in: 2013 IEEE International Conference on Robotics and Automation, 2013, pp. 5600–5605, http://dx.doi.org/10.1109/ICRA.2013.6631381.

[32] W. Dong, K. Sheng, B. Huang, K. Xiong, K. Liu, X. Cheng, Stretchable self-powered TENG sensor array for human-robot interaction based on conductive ionic gels and LSTM neural network, IEEE Sensors J. 24 (22) (2024) 37962–37969, http://dx.doi.org/10.1109/JSEN.2024.3464633.

[33] H. Wang, H. Wu, D. Ye, C. Zhao, Q. Wu, S. Wang, Z. Zhang, M. Zeng, H. Wei, Y. Huang, Micro-cylindrical/fibric electronic devices: materials, fabrication, health and environmental monitoring, Soft Sci. 4 (4) (2024) 41, http://dx.doi.org/10.20517/ss.2024.53.

[34] G. Kouros, I. Kotavelis, E. Skartados, D. Giakoumis, D. Tzovaras, A. Simi, G. Manacorda, 3D underground mapping with a mobile robot and a GPR antenna, in: 2018 IEEE/RSJ International Conference on Intelligent Robots and Systems, IROS, 2018, pp. 3218–3224, http://dx.doi.org/10.1109/IROS.2018.8593848.

[35] B. Coxworth, Mole-inspired robot is designed to dig its way through other planets, 2020, https://newatlas.com/robotics/mole-bot-tunnelling-robot/.

[36] B. Park, H. Myung, Underground localization using dual magnetic field sequence measurement and pose graph SLAM for directional drilling, Meas. Sci. Technol. 25 (12) (2014) 125101, http://dx.doi.org/10.1088/0957-0233/25/12/125101.

[37] B. Park, H. Myung, Resilient underground localization using magnetic field anomalies for drilling environment, IEEE Trans. Ind. Electron. 65 (2) (2018) 1377–1387, http://dx.doi.org/10.1109/TIE.2017.2733420.

[38] W.S. You, B.J. Choi, H.R. Choi, J.C. Koo, H. Moon, Localization using magnetic patterns for autonomous mobile robot, Int. J. Adv. Robot. Syst. 11 (3) (2014) 50, http://dx.doi.org/10.5772/57517.

[39] T. Zhang, H. Wei, H. Zheng, Z. Liang, H. Yang, Y. Zhang, H. Zhu, Y. Guan, X. Ding, K. Wang, K. Xu, Mole-inspired robot burrowing with forelimbs for planetary soil exploration, Adv. Intell. Syst. 6 (6) (2024) 2300392, http://dx.doi.org/10.1002/aisy.202300392.

[40] H.E. Project, BADGER - RoBot for autonomous unDerGround trenchless operations, mapping and navigation, 2020, http://dx.doi.org/10.3030/731968, Deliverable D1.2 - Overall system functionalities and system specifications.

[41] A.M. Baracu, L.A. Dinu Gugoasa, Review—Recent advances in microfabrication, design and applications of amperometric sensors and biosensors, J. Electrochem. Soc. 168 (3) (2021) 037503, http://dx.doi.org/10.1149/1945-7111/abe8b6.

[42] M.S. Sumitha, T.S. Xavier, Recent advances in electrochemical biosensors – A brief review, Hybrid Adv. 2 (2023) 100023, http://dx.doi.org/10.1016/j.hybadv.2023.100023.

[43] N.S. Abdalla, M.A. Youssef, H. Algarni, N.S. Awwad, A.H. Kamel, All solid-state poly (vinyl chloride) membrane potentiometric sensor integrated with nano-beads imprinted polymers for sensitive and rapid detection of bispyribac herbicide as organic pollutant, Molecules 24 (4) (2019) 712, http://dx.doi.org/10.3390/molecules24040712.

[44] P.K. Gopi, B. Mutharani, S.M. Chen, T.W. Chen, G.E. Eldesoky, M.A. Ali, S.M. Wabaidur, F. Shaik, C.Y. Tzu, Electrochemical sensing base for hazardous herbicide aclonifen using gadolinium niobate (GdNbO4) nanoparticles-actual river water and soil sample analysis, Ecotoxicol. Environ. Safety 207 (2021) 111285, http://dx.doi.org/10.1016/j.ecoenv.2020.111285.

[45] K. Prabhu, S.J. Malode, N.P. Shetti, Carbon-based electrochemical sensor for the detection and degradation of persistent toxic carbendazim in soil and water sample, Electrocatalysis 14 (1) (2023) 88–97, http://dx.doi.org/10.1007/s12678-022-00777-9.

[46] J. Dalmieda, P. Kruse, Metal cation detection in drinking water, Sensors 19 (23) (2019) 5134, http://dx.doi.org/10.3390/s19235134.

[47] G. Lisak, Reliable environmental trace heavy metal analysis with potentiometric ion sensors - reality or a distant dream, Environ. Pollut. 289 (2021) 117882, http://dx.doi.org/10.1016/j.envpol.2021.117882.

[48] V. Reyes-Loaiza, J.D.L. Roche, E. Hernandez-Renjifo, O. Idárraga, M.D. Silva, D.P. Valencia, T. Ghneim-Herrera, A. Jaramillo-Botero, Laser-induced graphene electrochemical sensor for quantitative detection of phytotoxic aluminum ions (Al_3^+) in soils extracts, Sci. Rep. 14 (1) (2024) 5772, http://dx.doi.org/10.1038/s41598-024-56212-0.

[49] A.H. Kamel, A.E.-G.E. Amr, N.S. Abdalla, M. El-Naggar, M.A. Al-Omar, A.A. Almehizia, Modified screen-printed potentiometric sensors based on man-tailored biomimetics for diquat herbicide determination, Int. J. Environ. Res. Public Heal. 17 (4) (2020) 1138, http://dx.doi.org/10.3390/ijerph17041138.

[50] M.F. Abdel-Ghany, L.A. Hussein, N.F.E. Azab, Novel potentiometric sensors for the determination of the dinotefuran insecticide residue levels in cucumber and soil samples, Talanta 164 (2017) 518–528, http://dx.doi.org/10.1016/j.talanta.2016.12.019.

[51] P.K. Gopi, B. Mutharani, S.M. Chen, R. Saraswathi, S.M. Chen, V. Mani, Electrochemical sensing base for hazardous herbicide aclonifen using gadolinium niobate ($GdNbO_4$) nanoparticles-actual river water and soil sample analysis, Ecotoxicol. Environ. Safety 207 (2021) 111285, http://dx.doi.org/10.1016/j.ecoenv.2020.111285.

[52] J.-H. Hwang, P. Pathak, X. Wang, K.L. Rodriguez, J. Park, H.J. Cho, W.H. Lee, A novel Fe-Chitosan-coated carbon electrode sensor for in situ As(III) detection in mining wastewater and soil leachate, Sensors Actuators B: Chem. 294 (2019) 89–97, http://dx.doi.org/10.1016/j.snb.2019.05.044.

[53] Z. Zhang, H. Karimi-Maleh, In situ synthesis of label-free electrochemical aptasensor-based sandwich-like AuNPs/PPy/Ti3C2Tx for ultrasensitive detection of lead ions as hazardous pollutants in environmental fluids, Chemosphere 324 (2023) 138302, http://dx.doi.org/10.1016/j.chemosphere.2023.138302.

[54] Y. Liu, X. Zeng, G.I.N. Waterhouse, X. Jiang, Z. Zhang, L. Yu, Potential stability improvement in Pb2+ ion selective electrodes by applying hydrophobic polyaniline as ion-to-electron transducer, Synth. Met. 281 (2021) 116898, http://dx.doi.org/10.1016/j.synthmet.2021.116898.

[55] M.A. Ali, C. Hu, K. Jahan, B. Yuan, M.S. Saleh, E. Ju, S. Gao, R. Panat, W.R. Heineman, V. Shanov, et al., Microfluidic impedimetric sensor for soil nitrate detection using graphene oxide and conductive nanofibers enabled sensing interface, Sensors Actuators B: Chem. 239 (2017) 1289–1299, http://dx.doi.org/10.1016/j.snb.2016.09.101.

[56] N.T. Garland, C. De Dobbelaere, B.D. Atkinson, K.S. McCarter, X. Guo, X. Pan, I. Papautsky, J. Cuppoletti, W.R. Heineman, V. Shanov, et al., Flexible laser-induced graphene for nitrogen sensing in soil, ACS Appl. Mater. Interfaces 10 (45) (2018) 39124–39133, http://dx.doi.org/10.1021/acsami.8b10991.

[57] R.K.A. Amali, H.N. Lim, I. Ibrahim, Z. Zainal, S.A.A. Ahmad, Silver nanoparticles-loaded copper (II)-terephthalate framework nanocomposite as a screen-printed carbon electrode modifier for amperometric nitrate detection, J. Electroanal. Chem. 918 (2022) 116440, http://dx.doi.org/10.1016/j.jelechem.2022.116440.

[58] G. Zhao, Y. Si, H. Wang, G. Liu, A portable electrochemical detection system based on graphene/ionic liquid modified screen-printed electrode for the detection of cadmium in soil by square wave anodic stripping voltammetry, Sensors 11 (1) (2023) 54–64, http://dx.doi.org/10.1016/S1452-3981(23)15826-3.

[59] N. Liu, G. Zhao, G. Liu, Sensitive stripping voltammetric determination of Pb (II) in soil using a Bi/single-walled carbon nanotubes-Nafion/ionic liquid nanocomposite modified screen-printed electrode, Int. J. Electrochem. Sci. 15 (8) (2020) 7868–7882, http://dx.doi.org/10.20964/2020.08.99.

[60] P.R. Villas-Boas, M.A.d. Franco, L. Martin-Neto, H.T. Gollany, D.M.B.P. Milori, Applications of laser-induced breakdown spectroscopy for soil characterization, part II: Review of elemental analysis and soil classification, Eur. J. Soil Sci. 71 (5) (2020) 805–818, http://dx.doi.org/10.1111/ejss.12889.

[61] M. Vitiello, Ultrashort Pulsed Laser Ablation of Solid Targets (Ph.D. thesis), 2005.

[62] H.-L. Zhao, L.-L. Cai, G. Wu, On polarization resolved laser induced breakdown spectroscopy combined with support-vector regression to improve the accuracy of soil heavy-metal (Cd) detection, Chin. J. Anal. Chem. 51 (2) (2023) 100176, http://dx.doi.org/10.1016/j.cjac.2022.100176.

[63] D.A. Cremers, L.J. Radziemski, Handbook of Laser-Induced Breakdown Spectroscopy, John Wiley & Sons, 2013.

[64] G.S. Senesi, N. Senesi, Laser-induced breakdown spectroscopy (LIBS) to measure quantitatively soil carbon with emphasis on soil organic carbon. A review, Anal. Chim. Acta 938 (2016) 7–17, http://dx.doi.org/10.1016/j.aca.2016.07.039.

[65] F.N. Mikkelsted, D. Adén, T. Nikolajsen, K.H. Laursen, A novel LIBS method for quantitative and high-throughput analysis of macro- and micronutrients in plants, J. Anal. At. Spectrom. 39 (2024) 2008–2020, http://dx.doi.org/10.1039/D4JA00105B.

[66] D. Díaz, D.W. Hahn, A. Molina, Evaluation of laser-induced breakdown spectroscopy (LIBS) as a measurement technique for evaluation of total elemental concentration in soils, Appl. Spectrosc. 66 (1) (2012) 99–106, http://dx.doi.org/10.1366/11-06349.

[67] R. Zhou, K. Liu, Z. Tang, Z. Hao, X. Li, X. Zeng, Determination of micronutrient elements in soil using laser-induced breakdown spectroscopy assisted by laser-induced fluorescence, J. Anal. At. Spectrom. 36 (3) (2021) 614–621, http://dx.doi.org/10.1039/D0JA00527D.

[68] Y. Xu, B. Han, X. Tan, Q. Jiao, Z. Ma, B. Lv, Y. Li, H. Li, Y. Zou, L. Yang, Establishment and evaluation of a quantitative analysis model for potentially toxic metals in wet soil samples by LIBS, Eur. J. Soil Sci. 73 (2) (2022) e13213, http://dx.doi.org/10.1111/ejss.13213.

[69] M. Dell'Aglio, R. Gaudiuso, R. Alrifai, A.D. Giacomo, Monitoring of Cr, Cu, Pb, V and Zn in polluted soils by laser induced breakdown spectroscopy (LIBS), JEM 13 (5) (2011) 1422–1428, http://dx.doi.org/10.1039/c0em00780c.

[70] Z. Yang, J. Ren, M. Du, Y. Zhao, K. Yu, Enhanced laser-induced breakdown spectroscopy for heavy metal detection in agriculture: A review, Sensors 22 (15) (2022) 5679, http://dx.doi.org/10.3390/s22155679.

[71] M. Ma, L. Fang, N. Zhao, X. Ma, Detection of cadmium and lead heavy metals in soil samples by portable laser-induced breakdown spectroscopy, Chemosensors 12 (3) (2024) 40, http://dx.doi.org/10.3390/chemosensors12030040.

[72] Y. Gou, X. Fu, S. Zhao, P. He, C. Zhao, G. Li, Improved convolutional neural network-assisted laser-induced breakdown spectroscopy for identification of soil contamination types, Spectrochim. Acta Part B: At. Spectrosc. 215 (2024) 106910, http://dx.doi.org/10.1016/j.sab.2024.106910.

[73] Y. Zhao, M.L. Guindo, X. Xu, M. Sun, J. Peng, F. Liu, Y. He, Deep learning associated with laser-induced breakdown spectroscopy (LIBS) for the prediction of lead in soil, Appl. Spectrosc. 73 (5) (2019) 565–573, http://dx.doi.org/10.1177/0003702819826283.

[74] Z. Wang, S. Xiao, C. Reuben, Q. Wang, J. Wang, Soil NOx emission prediction via recurrent neural networks, Comput. Mater. Contin. 77 (1) (2023) 285–297, http://dx.doi.org/10.32604/cmc.2023.044366.

[75] Y. Huang, S.S. Harilal, A. Bais, A.E. Hussein, Progress toward machine learning methodologies for laser-induced breakdown spectroscopy with an emphasis on soil analysis, IEEE Trans. Plasma Sci. 51 (7) (2023) 1729–1749, http://dx.doi.org/10.1109/TPS.2022.3231985.

[76] A. Wangeci, D. Adén, T. Nikolajsen, M.H. Greve, M. Knadel, Comparing laser-induced breakdown spectroscopy and visible near-infrared spectroscopy for predicting soil properties: A pan-European study, Geoderma 444 (2024) 116865, http://dx.doi.org/10.1016/j.geoderma.2024.116865.

[77] B.E. Madari, J.B. Reeves, P.L.O.A. Machado, C.M. Guimarães, E. Torres, G.W. McCarty, Mid- and near-infrared spectroscopic assessment of soil compositional parameters and structural indices in two ferralsols, Geoderma 136 (1–2) (2006) 245–259, http://dx.doi.org/10.1016/j.geoderma.2006.03.026.

[78] B. Tan, W. You, S. Tian, T. Xiao, M. Wang, B. Zheng, L. Luo, Soil nitrogen content detection based on near-infrared spectroscopy, Sensors 22 (20) (2022) 8013, http://dx.doi.org/10.3390/s22208013.

[79] C. Piccini, K. Metzger, G. Debaene, B. Stenberg, S. Götzinger, L. Borůvka, T. Sandén, L. Bragazza, F. Liebisch, In-field soil spectroscopy in Vis–NIR range for fast and reliable soil analysis: A review, Eur. J. Soil Sci. 75 (2) (2024) e13481, http://dx.doi.org/10.1111/ejss.13481.

[80] P. Kühn, T. Proß, C. Römermann, K. Wesche, H. Bruelheide, Using near-infrared spectroscopy to predict nitrogen and phosphorus concentrations of herbarium specimens under different storage conditions, Plant Methods 20 (1) (2024) 19, http://dx.doi.org/10.1186/s13007-024-01146-x.

[81] L. Wei, J. Yuan, Y. Wang, Y. Zhang, Y. Zhao, Y. Chen, J. Zhang, Y. Liu, Y. Wang, Y. Zhang, Hyperspectral inversion of soil organic matter content based on a combined spectral index model, Sensors 20 (10) (2020) 2777, http://dx.doi.org/10.3390/s20102777.

[82] H. Liu, H. Mao, W. Zhu, X. Zhang, H. Gao, Rapid diagnosis of tomato N-P-K nutrition level based on hyperspectral technology, Trans. Chin. Soc. Agric. Eng. 31 (S1) (2015) 212–220, http://dx.doi.org/10.3969/j.issn.1002-6819.2015.z1.025.

[83] D. Xu, S. Chen, Y. Zhou, W. Ji, Z. Shi, Spatial estimation of soil organic matter and total nitrogen by fusing field Vis–NIR spectroscopy and multispectral remote sensing data, Remote. Sens. 17 (4) (2025) 729, http://dx.doi.org/10.3390/rs17040729.

[84] S. Krzebietke, M. Daszykowski, H. Czarnik-Matusewicz, I. Stanimirova, L. Pieszczek, S. Sienkiewicz, J. Wierzbowska, Monitoring the concentrations of Cd, Cu, Pb, Ni, Cr, Zn, Mn and Fe in cultivated Haplic Luvisol soils using near-infrared reflectance spectroscopy and chemometrics, Talanta 251 (2023) 123749, http://dx.doi.org/10.1016/j.talanta.2022.123749.

[85] G. Siebielec, G.W. McCarty, T.I. Stuczynski, J.B. Reeves, Near- and mid-infrared diffuse reflectance spectroscopy for measuring soil metal content, J. Environ. Qual. 33 (6) (2004) 2056–2069, http://dx.doi.org/10.2134/jeq2004.2056.

[86] B. Guo, B. Zhang, Y. Su, D. Zhang, Y. Wang, Y. Bian, L. Suo, X. Guo, H. Bai, Retrieving zinc concentrations in topsoil with reflectance spectroscopy at opencast coal mine sites, Sci. Rep. 11 (1) (2021) 19909, http://dx.doi.org/10.1038/s41598-021-99106-1.

[87] S. Nawar, E.S. Mohamed, S. Essam-Eldeen Sayed, W.S. Mohamed, N.Y. Rebouh, A.A. Hammam, Estimation of key potentially toxic elements in arid agricultural soils using Vis-NIR spectroscopy with variable selection and PLSR algorithms, Front. Environ. Sci. 11 (2023) http://dx.doi.org/10.3389/fenvs.2023.1222871.

[88] S. Zhang, L. Shen, Y. Ren, Z. Li, X. Chen, X. Wang, VNIR estimation of heavy metals concentrations in suburban soil with multi-scale geographically weighted regression, Catena 219 (2022) 106585, http://dx.doi.org/10.1016/j.catena.2022.106585.

[89] L. Zhong, X. Xu, W. Zhao, Y. Chen, X. Li, Y. Zhang, Indirect estimation of heavy metal contamination in rice soil using spectral techniques, Plants 13 (6) (2024) 831, http://dx.doi.org/10.3390/plants13060831.

[90] J. Liu, Y. Zhang, H. Wang, Y. Du, Study on the prediction of soil heavy metal elements content based on visible near-infrared spectroscopy, Spectrochim. Acta Part A: Mol. Biomol. Spectrosc. 199 (2018) 43–49, http://dx.doi.org/10.1016/j.saa.2018.03.040.

[91] A. Haghighizadeh, F. Moore, P. Keshavarzi, B. Keshavarzi, Comprehensive analysis of heavy metal soil contamination in mining environments: Impacts, monitoring techniques, and remediation strategies, Arab. J. Chem. 17 (6) (2024) 105777, http://dx.doi.org/10.1016/j.arabjc.2024.105777.

[92] F. Shubitidze, K. O'Neill, K. Sun, K.D. Paulsen, Investigation of broadband electromagnetic induction scattering by highly conductive, permeable, arbitrarily shaped 3-D objects, IEEE Trans. Geosci. Remote Sens. 42 (3) (2004) 540–556, http://dx.doi.org/10.1109/TGRS.2003.821699.

[93] C.A. Charalambous, A. Demetriou, A.L. Lazari, A.I. Nikolaidis, Effects of electromagnetic interference on underground pipelines caused by the operation of high voltage AC traction systems: The impact of harmonics, IEEE Trans. Power Deliv. 33 (6) (2018) 2664–2672, http://dx.doi.org/10.1109/TPWRD.2018.2803080.

[94] G. Betta, D. Capriglione, L. Ferrigno, G. Miele, Influence of Wi-Fi computer interfaces on measurement apparatuses, IEEE Trans. Instrum. Meas. 59 (12) (2010) 3244–3252, http://dx.doi.org/10.1109/TIM.2010.2047303.

[95] A.G. Martins-Britto, T.A. Papadopoulos, A.I. Chrysochos, Transient electromagnetic interference between overhead and underground conductors, IEEE Trans. Electromagn. Compat. 66 (3) (2024) 983–992, http://dx.doi.org/10.1109/TEMC.2024.3376971.

[96] D. Chrysostomou, A. Dimitriou, N.D. Kokkinos, C.A. Charalambous, Short-term electromagnetic interference on a buried gas pipeline caused by critical fault events of a wind park: A realistic case study, IEEE Trans. Ind. Appl. 56 (2) (2020) 1162–1170, http://dx.doi.org/10.1109/TIA.2020.2965494.

[97] D. Stet, D.D. Micu, L. Czumbil, B. Manea, Case studies on electromagnetic interference between HVPL and buried pipelines, in: 2014 International Conference on Electrical Power and Energy Systems, ICEPES, 2014, pp. 231–236, http://dx.doi.org/10.1109/ICEPE.2014.6969903.

[98] M. Alexandru, L. Czumbil, D.D. Micu, T. Papadopoulos, Analysis of electromagnetic interferences between AC high voltage power lines and metallic pipeline using two different approaches based on circuit theory and electromagnetic field theory, in: 2020 11th International Conference and Exposition on Electrical and Power Engineering, EPE, 2020, pp. 519–524, http://dx.doi.org/10.1109/EPE50722.2020.9305583.

[99] M. Paolone, C.A. Nucci, E. Petrache, F. Rachidi, Lightning induced disturbances in buried cables—Part II: Experiment and model validation, IEEE Trans. Electromagn. Compat. 47 (3) (2005) 509–520, http://dx.doi.org/10.1109/TEMC.2005.853163.

[100] H. Chen, M. Zhang, Z. Tian, Radiated electromagnetic disturbance for the DC trolley locomotive system in underground coal mines, in: 2018 IEEE International Conference on Mechatronics and Automation, ICMA, 2018, pp. 210–214, http://dx.doi.org/10.1109/IMCEC.2018.8469190.

[101] T. Wang, J. Li, N. Liu, S. Peng, Y. Li, G. Fang, A new data processing method for magnetic anomaly detection and localization based on 2-D orthonormal basis functions, IEEE Trans. Geosci. Remote Sens. 61 (2023) 1–11, http://dx.doi.org/10.1109/TGRS.2023.3286862.

[102] L. Wang, S. Zhang, S. Chen, C. Luo, Underground target localization based on improved magnetic gradient tensor with towed transient electromagnetic sensor array, IEEE Access 10 (2022) 25025–25033, http://dx.doi.org/10.1109/ACCESS.2022.3156080.

[103] A. Srivastav, P. Nguyen, M. McConnell, K.A. Loparo, S. Mandal, A highly digital multiantenna ground-penetrating radar (GPR) system, IEEE Trans. Instrum. Meas. 69 (10) (2020) 7422–7436, http://dx.doi.org/10.1109/TIM.2020.2984415.

[104] A. Markham, N. Trigoni, D.W. Macdonald, S.A. Ellwood, Underground localization in 3-D using magneto-inductive tracking, IEEE Sensors J. 12 (6) (2012) 1809–1816, http://dx.doi.org/10.1109/JSEN.2011.2178064.

[105] L. Wang, S. Zhang, S. Chen, H. Jiang, Fast localization of underground targets by magnetic gradient tensor and Gaussian-Newton algorithm with a portable transient electromagnetic system, IEEE Access 9 (2021) 148469–148478, http://dx.doi.org/10.1109/ACCESS.2021.3124285.
[106] Z. Xu, W. Yang, K. You, W. Li, Y.-i. Kim, Vehicle autonomous localization in local area of coal mine tunnel based on vision sensors and ultrasonic sensors, PLoS One 12 (2017) 1–31, http://dx.doi.org/10.1371/journal.pone.0171012.
[107] J.P. Jordaan, C.P. Kruger, B.J. Silva, G.P. Hancke, An ultrasonic-based localization system for underground mines, in: 2017 IEEE 15th International Conference on Industrial Informatics, INDIN, 2017, pp. 141–146, http://dx.doi.org/10.1109/INDIN.2017.8104761.
[108] M. Jiang, Y. Song, Y. Li, Y. Yang, X. Xu, X. Xu, Underwater loop-closure detection for mechanical scanning imaging sonar by filtering the similarity matrix with probability hypothesis density filter, IEEE Access 7 (2019) 166614–166628, http://dx.doi.org/10.1109/ACCESS.2019.2952445.
[109] Z. Zhang, Y. Chen, X. Wang, Y. Li, X. Chen, J. Luo, A dual-mode 2D matrix array for ultrasound image-guided noninvasive therapy, IEEE Trans. Biomed. Eng. 68 (12) (2021) 3482–3490, http://dx.doi.org/10.1109/TBME.2021.3073951.
[110] A.V. Nikolaev, S.V. Zherdev, A.A. Sanina, D.A. Gaponov, S.A. Tereshchenko, Quantitative evaluation of an automated cone-based breast ultrasound scanner for MRI–3D US image fusion, IEEE Trans. Med. Imaging 40 (4) (2021) 1229–1239, http://dx.doi.org/10.1109/TMI.2021.3050525.
[111] M.A. Carpenter, Z. Zhang, Anelasticity maps for acoustic dissipation associated with phase transitions in minerals: Anelasticity maps for acoustic dissipation, Geophys. J. Int. 186 (1) (2011) 279–295, http://dx.doi.org/10.1111/j.1365-246X.2011.05028.x.
[112] J.J.S.D. Figueiredo, M.A. Schoenberg, J.A.T. Costa, M. Tygel, Shear wave anisotropy from aligned inclusions: ultrasonic frequency dependence of velocity and attenuation, Geophys. J. Int. 193 (1) (2013) 475–488, http://dx.doi.org/10.1093/gji/ggs130.
[113] N. Liu, R. Paranjape, K. Asghari, Underground ultrasound probing for monitoring carbon dioxide flooding in oil producing reservoirs, in: Proceedings of the 2002 IEEE Canadian Conference on Electrical and Computer Engineering, 2002, pp. 510–514, http://dx.doi.org/10.1109/CCECE.2002.1015279.
[114] A. Benedetto, L. Pajewski (Eds.), Civil Engineering Applications of Ground Penetrating Radar, Springer International Publishing, 2015, http://dx.doi.org/10.1007/978-3-319-04813-0.
[115] R. Persico, Introduction to Ground Penetrating Radar, Wiley, 2014, http://dx.doi.org/10.1002/9781118835647.
[116] Y. Qin, F. Wang, C. Zhou, A distributed UWB-based localization system in underground mines, J. Netw. 10 (3) (2015) 134–140, http://dx.doi.org/10.4304/jnw.10.3.134-140.
[117] Y. Qin, C. Zhou, S.-H. Yang, F. Wang, A distributed newton iteration based localization scheme in underground tunnels, in: 2012 UKACC International Conference on Control, 2012, pp. 851–856, http://dx.doi.org/10.1109/CONTROL.2012.6334743.
[118] A.E. Forooshani, S. Bashir, D.G. Michelson, S. Noghanian, A survey of wireless communications and propagation modeling in underground mines, IEEE Commun. Surv. Tutor. 15 (4) (2013) 1524–1545, http://dx.doi.org/10.1109/SURV.2013.031413.00130.
[119] S.-C. Lin, A.A. Alshehri, P. Wang, I.F. Akyildiz, Magnetic induction-based localization in randomly deployed wireless underground sensor networks, IEEE Internet Things J. 4 (5) (2017) 1454–1465, http://dx.doi.org/10.1109/JIOT.2017.2729887.
[120] Z. Sun, I.F. Akyildiz, Magnetic induction communications for wireless underground sensor networks, IEEE Trans. Antennas and Propagation 58 (7) (2010) 2426–2435, http://dx.doi.org/10.1109/TAP.2010.2048858.
[121] QuSpin, Total-field magnetometer, 2025, https://quspin.com/qtfm-gen-2/.
[122] QuSpin, Zero-field magnetometer, 2025, https://quspin.com/products-qzfm/.
[123] S.-C. Yeh, W.-H. Hsu, W.-Y. Lin, Y.-F. Wu, Study on an indoor positioning system using Earth's magnetic field, IEEE Trans. Instrum. Meas. 69 (3) (2020) 865–872, http://dx.doi.org/10.1109/TIM.2019.2905750.
[124] B. Li, T. Gallagher, A.G. Dempster, C. Rizos, How feasible is the use of magnetic field alone for indoor positioning? in: 2012 International Conference on Indoor Positioning and Indoor Navigation, IPIN, 2012, pp. 1–9, http://dx.doi.org/10.1109/IPIN.2012.6418880.
[125] G. Ouyang, K. Abed-Meraim, Analysis of magnetic field measurements for indoor positioning, Sensors 22 (11) (2022) 4014, http://dx.doi.org/10.3390/s22114014.
[126] G. Ouyang, K. Abed-Meraim, A survey of magnetic-field-based indoor localization, Electronics 11 (6) (2022) 864, http://dx.doi.org/10.3390/electronics11060864.
[127] H.-S. Kim, W. Seo, K.-R. Baek, Indoor positioning system using magnetic field map navigation and an encoder system, Sensors 17 (3) (2017) 651, http://dx.doi.org/10.3390/s17030651.
[128] H. Nicolas, T. Quirin, J. Pascal, FPGA-based magnetic field camera for dynamic magnetic field mapping, IEEE Sensors Lett. 8 (5) (2024) 1–4, http://dx.doi.org/10.1109/LSENS.2024.3389099.
[129] R. Savarapu, A. Sohan, P. Kollu, Fabrication advancements in integrated fluxgate sensors: A mini review, Adv. Eng. Mater. 24 (4) (2022) 2101040, http://dx.doi.org/10.1002/adem.202101040.
[130] H.S. Alpert, M.E. Rudinsky, S.V. Novikov, I.V. Sabinina, A.K. Gutakovskii, Effect of geometry on sensitivity and offset of AlGaN/GaN and InAlN/GaN hall-effect sensors, IEEE Sensors J. 19 (10) (2019) 3640–3646, http://dx.doi.org/10.1109/JSEN.2019.2895546.
[131] M.A. Khan, J. Sun, B. Li, A. Przybysz, J. Kosel, Magnetic sensors-A review and recent technologies, Eng. Res. Express 3 (2) (2021) 022005, http://dx.doi.org/10.1088/2631-8695/ac0838.
[132] Z. Zhenhong, O. Syuji, A. Osamu, K. Hideto, Development of the highly precise magnetic current sensor module of +/-300 a utilizing AMR element with bias-magnet, IEEE Trans. Magn. 51 (1) (2015) 1–5, http://dx.doi.org/10.1109/TMAG.2014.2359209.
[133] S. Lin, M. Lai, W. Fang, Using peacock shape anisotropic magnetoresistance (AMR) and Ni mushroom array to achieve tri-axis magnetic sensor, in: 2024 IEEE 37th International Conference on Micro Electro Mechanical Systems, MEMS, 2024, pp. 52–55, http://dx.doi.org/10.1109/MEMS58180.2024.10439533.
[134] I. Bolshakova, R. Holyaka, T. Marusenkova, A. Dzyuba, V. Yaskevich, Stability of gold nanofilms' based hall sensors under thermal loads typical for the DEMO ex-vessel environment, in: 2018 IEEE 15th International Conference on the Experience of Designing and Application of CAD Systems, CADSM, 2018, pp. 475–479, http://dx.doi.org/10.1109/TCSET.2018.8336244.
[135] Y. Sakuma, K. Takashima, T. Ohhira, H. Hashimoto, Magnetic absolute encoder with magnet of different magnetic flux densities and AMR sensors, in: 2023 49th Annual Conference of the IEEE Industrial Electronics Society, IECON, 2023, pp. 1–6, http://dx.doi.org/10.1109/IECON51785.2023.10312293.
[136] Allegro MicroSystems, From hall effect to TMR, 2003, https://www.allegromicro.com/-/media/files/application-notes/an117-from-hall-effect-to-tmr.pdf?sc_lang=en.
[137] C. Treutler, Magnetic sensors for automotive applications, Sensors Actuators A: Phys. 91 (1) (2001) 2–6, http://dx.doi.org/10.1016/S0924-4247(01)00621-5, Third European Conference on Magnetic Sensors & Actuators.
[138] S. Saha, K.B. Nandapurkar, A simple digitizer for GMR-based magnetic field sensor with some key practical considerations, IEEE Sensors J. 24 (10) (2024) 16290–16298, http://dx.doi.org/10.1109/JSEN.2024.3380606.
[139] Analog Devices, Integrated AMR angle sensor and signal conditioner ADA4571 - data sheet, 2014, https://www.analog.com/media/en/technical-documentation/data-sheets/ADA4571.pdf.
[140] K. Komuro, D. Oshima, T. Kato, Fabrication of GMR sensors with antiphase magnetization modulation and closed-loop operation, IEEE Trans. Magn. 59 (11) (2023) 1–5, http://dx.doi.org/10.1109/TMAG.2023.3284398.
[141] A.H. Khawaja, Q. Huang, L. Lian, Experimental study of tunnel and anisotropic magnetoresistive sensor for power system magnetic field measurement applications, in: 2015 IEEE International Conference on Smart Instrumentation, Measurement and Applications, ICSIMA, 2015, pp. 1–5, http://dx.doi.org/10.1109/ICSIMA.2015.7559007.
[142] M.S. Krishna, S. Singh, B.K. Kaushik, Edge tailored MgO nanoribbons for spintronics applications: A first principle investigations, IEEE Trans. Electron Devices 70 (7) (2023) 3551–3558, http://dx.doi.org/10.1109/TED.2023.3279802.
[143] L.V. Panina, K. Mohri, High-frequency giant magneto-impedance in Co-rich amorphous wires and films, J. Magn. Soc. Jpn. 19 (2) (1995) 265–268, http://dx.doi.org/10.3379/jmsjmag.19.265.
[144] D. Krause, M. Stahl-Offergeld, M. Sand, C. Kohlbrenner, R. Weigel, Sensor resistance based sensitivity temperature drift tracking of integrated 3D hall sensors, in: 2023 IEEE Sensors, 2023, pp. 1–4, http://dx.doi.org/10.1109/SENSORS56945.2023.10325285.
[145] Z. Zhenchuan, D. Xiusheng, L. Shengjun, Research progress of giant magneto-impedance (GMI) sensors, in: 2017 2nd International Conference on Frontiers of Sensors Technologies, ICFST, 2017, pp. 73–77, http://dx.doi.org/10.1109/ICFST.2017.8210476.
[146] A. Khatun, F. Bender, A.K. Mensah-Brown, F. Josse, Noninvasive monitoring of internal state of Li-ion batteries via magnetic sensing, IEEE Sensors J. 24 (3) (2024) 2637–2646, http://dx.doi.org/10.1109/JSEN.2023.3339441.
[147] G.D. Demin, B.V. Lobanov, N.A. Dyuzhev, Frequency analysis of the GMI effect in a thin-film magnetic structure with an insulator in the linear and nonlinear operating regimes, in: 2024 18th International Conference on Electron Devices and Materials, EDM, 2024, pp. 170–173, http://dx.doi.org/10.1109/EDM61683.2024.10615123.
[148] P. Ripka, Advances in fluxgate sensors, Sensors Actuators A: Phys. 106 (1–3) (2003) 8–14, http://dx.doi.org/10.1016/S0924-4247(03)00094-3.
[149] L. Perez, C. Aroca, P. Sánchez, E. López, M.C. Sánchez, Planar fluxgate sensor with an electrodeposited amorphous core, Sensors Actuators A: Phys. 109 (3) (2004) 208–211, http://dx.doi.org/10.1016/j.sna.2003.08.015.
[150] W.-S. Huang, C.-C. Lu, J.-T. Jeng, A novel 3D CMOS micro-fluxgate magnetic sensor for low magnetic field detection, in: 2010 IEEE SENSORS Conference, 2010, pp. 1791–1794, http://dx.doi.org/10.1109/ICSENS.2010.5689981.
[151] P. Ripka, New directions in fluxgate sensors, J. Magn. Magn. Mater. 215–216 (2000) 735–739, http://dx.doi.org/10.1016/S0304-8853(00)00273-0.
[152] Honeywell, Current Sensors CSNV700 Series, https://automation.honeywell.com/us/en/products/sensing-solutions/sensors/current-sensors/csnv700-series.

[153] LEM, Current Sensors CAB 1500-000 Series, https://www.lem.com/en/product-list/cab-1500000.
[154] N. Alberto, M.F. Domingues, C. Marques, P. André, P. Antunes, Optical fiber magnetic field sensors based on magnetic fluid: A review, Sensors 18 (12) (2018) 4325, http://dx.doi.org/10.3390/s18124325.
[155] W. Zhang, Z. Li, L. Xu, Y. Li, J. Yang, X. Zhang, Y. Wang, Advances in tapered optical fiber sensor structures: From conventional to novel and emerging, Biosensors 13 (6) (2023) 644, http://dx.doi.org/10.3390/bios13060644.
[156] Z.J. Liu, Y.G. Liu, Z. Wang, W. Huang, T. Han, Z. Li, An optical microfiber taper magnetic field sensor with temperature compensation, IEEE Sensors J. 15 (9) (2015) 4853–4856, http://dx.doi.org/10.1109/JSEN.2015.2429911.
[157] X.Q. Lei, B.J. Peng, D.R. Chen, Q.G. Shi, X.W. Ma, An all-fiber magnetic field sensor based on dual-s-shaped optic fiber integrated with magnetic fluid, IEEE Sensors J. 16 (4) (2016) 958–964, http://dx.doi.org/10.1109/JSEN.2015.2496402.
[158] T.M. Tierney, N. Holmes, S. Mellor, J.D. López, G. Roberts, R.M. Hill, E. Boto, J. Leggett, V. Shah, M.J. Brookes, R. Bowtell, G.R. Barnes, Optically pumped magnetometers: From quantum origins to multi-channel magnetoencephalography, NeuroImage 199 (2019) 598–608, http://dx.doi.org/10.1016/j.neuroimage.2019.05.063.
[159] R. Jiménez-Martínez, S. Knappe, Microfabricated optically-pumped magnetometers, in: A. Grosz, M.J. Haji-Sheikh, S.C. Mukhopadhyay (Eds.), High Sensitivity Magnetometers, Springer International Publishing, Cham, 2017, pp. 523–551, http://dx.doi.org/10.1007/978-3-319-34070-8_17.
[160] K. Jensen, P. Kehayias, D. Budker, Magnetometry with nitrogen-vacancy centers in diamond, in: A. Grosz, M.J. Haji-Sheikh, S.C. Mukhopadhyay (Eds.), High Sensitivity Magnetometers, Springer International Publishing, Cham, 2017, pp. 53–576, http://dx.doi.org/10.1007/978-3-319-34070-8_18.
[161] Q.ANT, Quantum magnetometer 10 (Q.M. 10), 2025, https://qant.com/magnetometer/.